

# Linear and Nonlinear Relations between Relative Plate Velocity and Seismicity

by P. Bird<sup>1</sup>, Y. Y. Kagan<sup>1</sup>, D. D. Jackson<sup>1</sup>, F. P. Schoenberg<sup>2</sup>, & M. J. Werner<sup>1,3</sup>

<sup>1</sup>Department of Earth and Space Sciences, UCLA

<sup>2</sup>Department of Statistics, UCLA

<sup>3</sup>Now at: Swiss Seismological Service, ETH Zurich

Revised version of 3 August 2009 for *BSSA*

*Corresponding author:*

Peter Bird

Department of Earth and Space Sciences

University of California

Los Angeles, CA 90095-1567

**[pbird@ess.ucla.edu](mailto:pbird@ess.ucla.edu)**

**Abstract.** Relationships between relative plate velocity and seismicity differ by plate boundary class. We test the null hypothesis of linearity of earthquake rates with velocity in each of 7 classes. A linear relationship is expected if earthquake rate is proportional to seismic moment rate, which is proportional to relative plate velocity. To reduce bias by aftershocks and swarms, we estimate independence probabilities of earthquakes and use them as weights. We assign shallow earthquakes to boundary steps and classes, then sort boundary steps within each class by velocity, and plot cumulative earthquakes against cumulative model moment rate. We use 2 measures of nonlinearity, and  $10^4$  stochastic simulations to assess significance. In subduction zones the relationship between seismicity and velocity is nonlinear with 99.9% confidence. Slower subduction at  $<66$  mm/a (producing 35% of tectonic moment under the null hypothesis) produces only 20% of subduction earthquakes. Continental convergent boundaries display

similar nonlinearity ( $P < 0.001$  for the null hypothesis). Ocean spreading ridges show seismicity decreasing with velocity. Oceanic transform faults and oceanic convergent boundaries show marginal nonlinearity ( $P < 0.01$ ;  $P < 0.05$ ). Continental rifts and continental transform faults follow the null hypothesis. Three effects may contribute to velocity-dependence in subduction: (1) The brittle/ductile transition at a critical temperature is advected deeper by faster underthrusting; (2) subducted sediment is viscous, so lower stresses in slower boundaries discourage earthquakes; (3) pore pressures increase with velocity, encouraging frictional failure. Mechanism (1) has only minor effects on earthquake productivity, but mechanisms (2) and (3) could be important.

### **Introduction**

Relative plate motion causes most shallow earthquakes. (Other causes including volcanism, slope failure, postglacial rebound, and thermal contraction of lithosphere may be locally more important, especially in plate interiors.) Many forecasts of future seismicity and/or seismic hazard incorporate consideration of relative plate motion, whether expressed as slip on discrete faults or as anelastic straining of a continuum (*e.g.*, Brune, 1968; Kostrov, 1974; Bird and Liu, 2007; Liu and Bird, 2008). While it is natural to expect some kind of proportionality between relative plate velocity and seismicity, there are at least 3 reasons to test this hypothesis critically.

First, Bird and Kagan (2004) found that most of the 7 different classes of plate boundary defined by Bird (2003) have different productivities for earthquakes and for seismic moment, which they interpreted as resulting from different “mean coupled thicknesses” of seismogenic lithosphere, ranging from 0.13 to 18 km. (Mean coupled thickness  $\langle cz \rangle$  is the mean value of the product of a dimensionless seismic coupling coefficient  $c$  with the depth range  $z$  within

which the lithosphere is potentially seismic.) Perhaps there are additional variations in coupled thickness which have not yet been recognized, especially since the physics determining coupling remain unclear.

Second, many authors (Solomon, 1976; Solomon and Burr, 1979; Frohlich and Apperson, 1992; Sobolev and Rundquist, 1999; Bird *et al.*, 2002; Kreemer *et al.*, 2002; Bird and Kagan, 2004) have found that normal-faulting seismicity of ocean spreading ridges actually declines with increasing velocity. Bird *et al.* (2002) also found declines in coupled thickness and in corner magnitude with increasing velocity of oceanic transform faults.

Third, there has been much discussion about possible linkages between maximum sizes of subduction earthquakes and subduction velocity, and/or age of the subducting plate. Ruff & Kanamori (1980, 1983) asserted that “characteristic maximum earthquake size” in subduction zones is positively correlated with relative plate velocity, and negatively correlated with age of the subducting plate. However, when Pacheco *et al.* (1993) attempted to measure the seismic coupling coefficients of individual subduction zones, they did not find any correlation with relative plate velocity, which raises doubt about the correlation with “characteristic maximum earthquake size” claimed by Ruff & Kanamori (1980, 1983). McCaffrey (1997a) argued that we don’t yet have enough data to reliably determine maximum earthquake sizes in specific subduction zones. McCaffrey (1997b) took the argument further by demonstrating that the correlation between earthquake counts and subduction velocity combines with the Gutenberg-Richter relation to explain the apparent correlation of maximum earthquake size with relative plate velocity that Ruff & Kanamori (1980, 1983) had noted. McCaffrey (1997b) also questioned the correlation of larger earthquakes with younger subducting lithosphere by showing that theoretically we should expect the opposite. Our view is that these controversies have

demonstrated the fragility of conclusions which are based on maximum earthquake sizes, as this feature of subduction zones is poorly displayed in the short available instrumental catalogs.

A related issue is whether degree of seismic coupling in subduction zones depends on the age of the subduction zone. Kanamori (1977) studied recent great subduction earthquakes and concluded that the Chile and Alaska subduction zones are strongly coupled, while the Sanriku and Kurile subduction zones are largely decoupled. Uyeda and Kanamori (1979) further proposed a natural progression in which each subduction zone changes from coupled to decoupled with age, altering the regional stress state and triggering back-arc spreading. Testing such hypotheses would be doubly difficult because we would first have to measure long-term-average coupling in single subduction zones, and then also infer their total histories of convergence. In most cases, this cannot be done from the record of seafloor magnetic anomalies, which extends back only to 170 Ma.

In this project we explicitly test the null hypothesis of a linear relation between present seismicity and present relative plate velocity within each of the 7 classes of plate boundary. The difference from our previous studies is that here we examine earthquake rate rather than moment rate. Moment rate is hard to estimate accurately from any short catalog because of: (a) the dominance of the moments of the largest earthquakes and (b) the insufficient sampling of the largest earthquakes from most classes of boundary. Instead, we quantify seismicity by rate of earthquakes above the completeness threshold magnitude of the catalog, a more stable measure. Thus, our null hypothesis of linearity in this project is the conjunction of two sub-hypotheses: (1) Moment rate will be proportional to plate velocity, because coupled thickness, fault dip, and elastic shear modulus are assumed constant within each boundary class; and (2) the earthquake rate will be proportional to moment rate because the shape of the frequency/magnitude relation is

assumed constant within each boundary class. It is not necessary to assume that this frequency/magnitude relation is a tapered Gutenberg-Richter distribution (Jackson & Kagan, 1999; Kagan & Jackson, 2000) or that the tapered Gutenberg-Richter parameters of spectral slope and corner magnitude inferred by Bird and Kagan (2004) are correct. One drawback to our new approach is that if the null hypothesis fails, we will not be certain whether the defect was in sub-hypothesis (1), or (2), or both. It will be necessary to invoke plausible (but nonunique) models of temperature, stress, and/or pore pressure to suggest revised relations between velocity, moment rate, and earthquake rate.

Although we believe earthquake counts to be more stable measures than moment sums, it is still true that a very long time window would be needed to get a reliable earthquake rate for any single fault. For example, the Cascadia trench (whose last great earthquake was 1700 AD) and the southern California section of the San Andreas fault (whose last great earthquake was 1857 AD) have each had low seismicity in the instrumental period. However, it is reasonable to suppose that in the decades following their last great earthquakes they also had abundant aftershocks, as seen in analogous settings in Sumatra and along the Denali fault today. To reduce the problems associated with short catalog time windows, we expand geographic scope to the greatest extent possible, and also look at the overall forms of cumulative seismicity distributions, rather than at details which may be based on the recent behaviors of single faults.

A final remaining question is whether the recent 25-year period in which  $m > 6$  earthquakes have been accurately and consistently recorded is adequate for testing linearity, even after averaging seismicity in subcatalogs of global extent. We will argue below that traditional statistical methods permit assigning confidence levels to all inferred cases of nonlinearity, assuming that we are able to decluster the catalog and work with the total numbers of

independent events. We could still be mistaken if there were undiscovered mechanisms for regional or global “super-clustering” of earthquakes (other than static and dynamic triggering and aftershock swarms). For example, it was once suspected that plate motions might be unsteady on decadal timescales, and that new space-geodesy methods would reveal this. Instead, it has been found (Stein, 1993; DeMets *et al.*, 2009) that plate velocities measured over decadal timescales by geodesy are usually consistent with velocities measured over 2-m.y. timescales using marine magnetic anomalies. If only a few plates have changed their velocities measurably in the last 2 Ma, then it is unlikely that changes in plate motion on century timescales are measurable or important.

### Computations

Our source catalog for this study is the Centroid Moment Tensor (CMT) catalog (Ekström *et al.*, 2005) formerly known as the Harvard CMT catalog but now known as the Global CMT catalog. It is available at <http://www.globalcmt.org/CMTsearch.html>. We use only shallow earthquakes, those whose nominal centroid depth is  $\leq 70$  km. We also limit the catalog in time (1982.01.01-2007.03.31) and by seismic moment ( $M > 2.07 \times 10^{17}$  to  $3.47 \times 10^{17}$  N m; equivalent to moment-magnitude limits of  $m > 5.51$  to 5.66) in order to assure that the subcatalogs we use are nearly complete (Kagan, 2003; Bird & Kagan, 2004). In this paper, we use the conversion:

$$m = (2/3)(\log_{10}(M) - 9.05) \quad (1)$$

of Hanks and Kanamori (1979). There is confusion because some authors have used slightly different values of the constant (Kagan, 2003). Magnitudes quoted in this paper (as a convenience for readers) should be converted to scalar moments using (1) only.

Because this study emphasizes earthquake counts rather than moment sums, we attempt to correct (to first order) for earthquake clustering in foreshock-mainshock-aftershock sequences,

so as to obtain rates more representative of long-term averages. To do this, we use maximum-likelihood fitting to determine the best-fitting parameters in the likelihood stochastic declustering model of Kagan (1991) as updated by Kagan *et al.* (2009). The latter paper provides all parameters in tables. The best-fitting branching model for global shallow seismicity then provides estimated probabilities that each earthquake was an independent event. The mean of these probabilities is 0.745 at threshold  $m_t = 5.55$ . In the rest of this study, we count earthquakes not as integers, but as fractions based on their individual independence probabilities (Kagan & Knopoff, 1976; Kagan & Jackson, 2000). This eliminates the need to decide exactly which events are aftershocks or other triggered seismicity.

The rationale for separating independent from dependent events is that the independent ones hypothetically result from tectonic strain accumulation only, while the dependent are at least partially caused by recent earthquakes. (We also examined results obtained without this weighting, and all are qualitatively the same.) The use of total independent events also simplifies our estimation of the significances of anomalies, as explained below.

Our plate-tectonic model for this study is the PB2002 model of Bird (2003), which includes estimated Euler poles of relative neotectonic rotation rate for 52 plates, estimated plate-boundary lines digitized as a sequence of small great-circle steps, and outlines of 13 “orogens” in which rigid-plate behavior is doubtful or unconstrained. In this study, we do not use any shallow earthquakes from within the 13 orogens of PB2002 because the lengthy process of kinematic modeling of each is still in progress. All plate-boundary steps in PB2002 were originally assigned, using objective criteria, to one of 7 classes of plate boundary (**Table 1**): Ocean Spreading Ridge (OSR), Oceanic Transform Fault (OTF), Oceanic Convergent Boundary (OCB), Subduction zone (SUB), Continental Rift Boundary (CRB), Continental Transform Fault

(CTF), or Continental Convergent Boundary (CCB). The individual locations, lengths, plate-boundary classes, and relative velocities of all plate-boundary steps are available in file PB2002\_steps.dat published by Bird (2003).

Shallow CMT earthquakes (from the complete part of the catalog, weighted by independence, and outside of orogens) are assigned to nearby plate-boundary steps of PB2002 by the algorithm of Bird & Kagan (2004). Relative probability that a particular earthquake was generated by a particular plate-boundary step is estimated as a product of factors for (1) intrinsic seismicity of that step; (2) geographic match; (3) match in orientation of the double-couple part of the moment tensor to one or more predefined model earthquakes for that step; (4) match of depth to the depth distribution of one or more predefined model earthquakes; and (5) a-priori relative probability of that (those) model earthquake(s) relative to others. The earthquake is assigned to the plate boundary step with the highest relative probability, and takes its plate-boundary class from that step. The earthquake counts resulting from this classification are shown in Table 1. Those shallow earthquakes which could not be assigned to a plate-boundary step (about 5% of those outside orogens) are considered intraplate, and are not used in this study.

After this classification process, we have an estimate of total independent earthquakes associated with each plate boundary step outside orogens. We also have the sum of the scalar moments of these events (also weighted by each event's independence probability). Scalar moment sums are not emphasized in this study, for reasons discussed above, but we present them in figures. Also, we have available the length and relative velocity of each plate-boundary step according to the PB2002 model. That makes it easy to compute a model tectonic moment rate for that step, using equation (11) of Bird & Kagan (2004) together with coupled thickness, fault-dip, and elastic-modulus parameters from Table 5 of that study.

The final step in our primary analysis is to collect all plate-boundary steps of one class (*e.g.*, Continental Transform Fault) and to sort them by relative plate velocity, from slow to fast. We then plot cumulative independent earthquake count as a fraction of the total earthquake count (ordinate) against cumulative tectonic moment rate as a fraction of the total tectonic moment rate (abscissa). These plots are displayed as **Figures 1-7**. Each occupies a unit square in dimensionless 2-D space, and displays a non-decreasing empirical function which is pinned at both the lower left (0, 0) and the upper right (1, 1). If our null hypothesis of linearity between plate motion and seismicity were correct, these plots should all approximate diagonal lines for each of the 7 plate boundary classes. The lower-left part of each curve is based on plate boundary steps with low relative velocities, and relative plate velocity increases to the right. Therefore, if coupled thickness of seismogenic lithosphere were actually increasing with relative plate velocity, then the curves would lie below the diagonal and display an overall concave-upward form. If coupled thickness of seismogenic lithosphere were actually decreasing with relative plate velocity, the curves would lie above the diagonal and display an overall convex-upward form.

Secondary analysis includes quantifying the departures of these curves from the diagonal, and estimating the significance of these departures. The Kolmogorov-Smirnov statistic for each plot treats the abscissa as free of variation, and measures departure from linearity as the greatest distance, measured vertically, between the empirical curve and the diagonal. Thus, it is a dimensionless number between 0 and 1. The Cramér-von-Mises statistic is the root-mean-square of the discrepancy (measured vertically) between the empirical curve and the diagonal, which is also a dimensionless number, but with range from 0 to  $\sqrt{1/3} \cong 0.577$ .

Because of finite-sample effects, the Kolmogorov-Smirnov and Cramér-von-Mises statistics will both vary from zero even under the null hypothesis. However, their expected sizes should decrease with the number of actual earthquakes assigned to the particular plate-boundary class under analysis (in proportion to the inverse square-root of the number) if the null hypothesis is correct. Thus, the significance of a particular value of each statistic increases with the number of earthquakes analyzed. To simulate the random fluctuations in these two statistics for the particular cases in question, we conducted 10,000 Monte-Carlo simulations of each plot, in each of which simulations the number of simulated independent earthquakes occurring on each plate-boundary step was an integer randomly sampled from a Poisson distribution based on the tectonic model prediction:

$$f(k; \lambda) = \frac{\lambda^k e^{-\lambda}}{k!} \quad (2)$$

where  $f(k; \lambda)$  is the probability that a random trial produces result  $k$  when the expectation is  $\lambda$ ;  $k$  is the non-negative integer representing the number of simulated independent earthquakes on that step in that simulation; and  $\lambda$  is the tectonic expectation for the number of independent earthquakes (varying across steps, but constant across simulations):  $\lambda = (\text{number of independent earthquakes for the plate-boundary class}) \times (\text{model tectonic moment rate for the plate-boundary step}) / (\text{sum of model tectonic moment rates for all steps})$ . At the end of each simulation we renormalize the earthquake counts (because the simulated totals are always slightly different from the target total) and then compute both Kolmogorov-Smirnov and Cramér-von-Mises statistics. After 10,000 simulations, we sort the simulated statistics by size and assign 5% exceedance probability to values exceeded only 500 times, 1% exceedance probability to values exceeded only 100 times, 0.1% exceedance probability to values exceeded only 10 times, and so

on. In this way, we determine the probability  $P$  that a particular value of the statistic (from a test with real data) might be equaled or exceeded due to random fluctuations in samples of modest size.

### **Interpretation**

When interpreting our results, we consider Kolmogorov-Smirnov and Cramér-von-Mises statistics whose values have exceedance probabilities  $P < 0.05$  under the null hypothesis as a minimum or necessary criterion for rejecting the null hypothesis of a linear relation between plate velocity and seismicity. However, they are not a sufficient condition, because we are also conscious that there are probably some systematic errors in the Euler poles of PB2002 and/or in the declustering of earthquakes (*et cetera*) which may cause small deviations of our empirical curves from the diagonal, but which are not considered in such statistics.

#### Boundaries with linear seismicity/velocity relations: Continental Transform Faults and Continental Rift Boundaries

In the classification of Bird (2003), “continental” lithosphere is that which lacks linear magnetic anomaly bands, and underlies land or shallow ocean with depth of less than 2 km. Continental Transform Faults (CTFs) are those plate boundary steps in continental lithosphere which have relative plate velocity vectors (based on model Euler poles) aligned within  $\pm 20^\circ$  of the azimuth of the plate boundary step. (This tolerance was included in the definition because both the Euler poles and the digitized plate boundary steps include small errors.)

The dimensionless seismicity/velocity plot for CTFs is shown as **Figure 1**. It is based on 230 earthquakes exceeding  $M_t = 3.47 \times 10^{17}$  N m ( $m_t = 5.66$ ), for which the sum of the independence probabilities is 173.9. The empirical curve of cumulative independent earthquake count outside orogens (as a fraction of total) versus cumulative model tectonic moment outside

orogens (as a fraction of total), when both are sorted and ordered from slow faults to fast faults, is quite close to the reference diagonal line representing the null hypothesis of linearity. The Kolomogorov-Smirnov statistic is 0.0782 ( $P \cong 0.26$ ) and the Cramér-von-Mises statistic is 0.0305 ( $P \cong 0.41$ ), so neither is significant.

It is notable that the empirical curve of cumulative (independent) earthquake moments for this boundary class is far less linear (Figure 1). This is because ~80% of the scalar moment occurred in the 4 largest earthquakes in this subcatalog. Even if they had fallen onto plate boundary steps evenly spaced along the abscissa, some nonlinearity would have been produced by these large steps. Computing significance of K-S and C-v-M statistics for this moment curve would be more complex because it would involve assumptions about the frequency/magnitude relation; furthermore, it is likely that the effective sample size would be only about 6~10 in a test based on moment sums. Therefore, we will display these cumulative moment curves for all plate boundary classes as supplemental information, but we will be cautious about interpreting them.

Continental Rift Boundaries (CRBs) in the classification of Bird (2003) are plate boundary steps in continental lithosphere with divergent relative plate motions, which includes both cases of high-angle normal faulting and low-angle detachment faulting. The dimensionless seismicity/velocity plot for CTFs is shown as **Figure 2**. It is based on a similar-sized sample of 214 earthquakes outside orogens exceeding  $M_t = 3.47 \times 10^{17}$  N m ( $m_t = 5.66$ ), for which the sum of the independence probabilities is 172.1. Again, the empirical curve of cumulative independent earthquake count is close to the reference diagonal. The Kolomogorov-Smirnov statistic is 0.0734 ( $P \cong 0.33$ ) and the Cramér-von-Mises statistic is 0.0399 ( $P \cong 0.21$ ), so neither is significant.

Both results are consistent with the null hypothesis of this paper, that earthquake production is linearly proportional to relative plate velocity. The simplest explanation would be that coupled thickness of seismogenic lithosphere ( $\langle cz \rangle$  of Bird & Kagan, 2004) is independent of velocity in each of these plate boundary classes, and that each has a frequency/magnitude distribution which is also independent of plate velocity. This general linearity in continental transtensional settings should simplify the forecasting of seismicity and seismic hazard in settings such as the Basin and Range province of the western United States, the Baikal rift, or the East Africa rift.

#### Marginally nonlinear relations: Oceanic Transform Faults and Oceanic Convergent Boundaries

“Oceanic” lithosphere either underlies ocean depths exceeding 2 km, or has linear magnetic anomaly bands (as in Iceland). Oceanic Transform Faults (OTFs) are those plate boundary steps in oceanic lithosphere which have relative plate velocity vectors (based on model Euler poles) aligned within  $\pm 20^\circ$  of the azimuth of the plate boundary step. We have studied seismicity of OTFs twice before, focusing on moment production and corner magnitudes rather than on earthquake counts. In Bird *et al.* (2002) we found that corner magnitude of OTFs appears to decrease from about 7.1 to about 6.3 as relative plate velocity increases, and that mean coupled thickness of seismogenic lithosphere declines quasi-exponentially with velocity, from about 3 km to 0.3 km. In Bird & Kagan (2004) we used a sample that was 40% larger, and found that when this seismic subcatalog is divided into 3 equal-sized pieces based on relative plate velocity, the slowest group had corner magnitude exceeding 7.4 (probably  $\sim 8$ ) while the intermediate and fast groups had corner magnitudes of about 6.5. Consistent with this, we also found that  $\langle cz \rangle$  is an order-of-magnitude larger for the slow group of OTFs than for the intermediate and fast groups (Table 5 of Bird & Kagan, 2004).

Despite these previous results, we assume uniform  $\langle cz \rangle$  for all OTFs when computing the model tectonic moment rates along the abscissa in **Figure 3**. (Because of the normalization of tectonic moment rates, it is not important what particular value is used.) The resulting empirical curve of cumulative independent earthquake count versus cumulative model tectonic moment is surprisingly linear. The cumulative moment curve is very nonlinear due to two very large earthquakes in the slow-OTF velocity category. Now, we had noted previously (Bird & Kagan, 2004) that these very large earthquakes appear to be outliers relative to a main earthquake population which is similar to the seismicity of intermediate and fast OTFs. This new result supports that concern. To first order, it appears that earthquake nucleation and growth up to our assumed threshold moment  $M_t = 2.07 \times 10^{17}$  N m ( $m_t = 5.51$ ) is proportional to relative plate velocity, but that a small fraction of the earthquakes on slow OTFs grow to very large sizes by some process that evades normal (tapered) Gutenberg-Richter frequency/magnitude scaling. Such outliers have not been seen (during the instrumental seismology time window) on any intermediate or fast OTFs, but perhaps this is just a coincidence, because their numbers are small (6  $m > 7.2$  earthquakes on all OTFs in 103 years, per Bird & Kagan, 2004). Fortunately, our present method of using independent earthquake counts (rather than moment sums) is hardly affected by a few such outlier events (Kreemer *et al.*, 2002).

The number of earthquakes in our sample of OTFs is quite large: 1285, for which the sum of the independence probabilities is 1193.1. Therefore, the formal significance of modest values of the K-S and C-v-M statistics is high. The K-S statistic for the cumulative independent earthquake count curve is 0.0534 ( $P = 0.002$ ) and the C-v-M statistic is 0.0261 ( $P = 0.007$ ). Both are formally significant, yet this small departure from linearity is difficult to interpret physically because of the complex form of the curve. We believe that future research on OTF seismicity

should focus on the circumstances responsible for the continued growth of the very large “outlier” events, rather than possible (but very subtle) departures from linearity in earthquake nucleation and growth to threshold size.

Oceanic Convergent Boundaries (OCBs) are a class of plate boundary defined by Bird (2003) for those cases of plate convergence in oceanic lithosphere without clear evidence of subduction (*i.e.*, no Quaternary volcano and no Wadati-Benioff zone of intermediate-depth seismicity). They may differ from Subduction zones (SUB) due to relatively small net fault slip, which has not yet brought oceanic sediment down into most of the seismogenic depth range. This type of plate boundary is relatively rare, and the sample of associated earthquakes is small: 101 in nonorogenic regions above  $M_t = 3.47 \times 10^{17}$  N m ( $m_t = 5.66$ ) in the CMT catalog, for which the sum of the independence probabilities is 86.6. The empirical cumulative independent earthquake count is plotted against cumulative model tectonic moment rate in **Figure 4**. The K-S statistic for this curve is 0.1571 ( $P = 0.03$ ), which is formally significant. However, the C-v-M statistic is 0.0684 ( $P = 0.07$ ), which is not. We are not convinced that any departure from the null hypothesis has been demonstrated, particularly because this cumulative-earthquake curve departs from linearity primarily in one dominant step upwards at cumulative tectonic moment rate of 80.2%, which results from a cluster of earthquakes (with sum of independence probabilities 12.7) on a single plate-boundary step.

One potential cause of a clustering artifact is that this particular OCB plate boundary step (on the SU-BH plate boundary around 127°E, 2.3°N) is immediately adjacent to SUB steps in the Molucca Passage. Therefore, some of the strong SUB seismicity may have “leaked” from one plate boundary step to a neighbor, and may have been mis-classified as OCB seismicity in this case. Also, it should be considered that no other authors have defined and mapped OCBs, and

that their map pattern in model PB2002 is therefore particularly likely to be incomplete or erroneous. Potentially, additional future information regarding the plate boundary step in question may cause it to be reclassified from OCB to SUB.

#### More earthquakes at low velocities: Oceanic Spreading Ridges

It is well-known that Oceanic Spreading Ridges (OSRs) have higher seismicity at low spreading rates, both in relative and in absolute terms (Solomon, 1976; Solomon and Burr, 1979; Frohlich and Apperson, 1992; Sobolev and Rundquist, 1999; Bird *et al.*, 2002; Kreemer *et al.*, 2002; Bird and Kagan, 2004). This can be seen by comparing a map of normal-faulting earthquakes on the slow Mid-Atlantic Ridge vs. the fast East Pacific Rise (*e.g.*, Fig. 2 in Bird *et al.*, 2002). **Figure 5** displays this nonlinearity very clearly: the convex-upward form of the curve means that earthquake productivity (earthquakes per unit of model tectonic moment) is greater when spreading is slow. The K-S statistic is 0.480 and the C-v-M statistic is 0.325; both lie far outside the range that we found in 10,000 Monte-Carlo simulations of the null hypothesis (for this subcatalog size and plate boundary geometry), so both have probabilities of exceedance  $P \ll 0.0001$  under the null hypothesis, which is rejected.

It is interesting that for this plate boundary class (only) the curve of cumulative independent scalar moment is nearly parallel to the curve of cumulative independent earthquake count. This is because the threshold magnitude  $m_t = 5.51$  ( $M_t = 2.07 \times 10^{17}$  N m) that we assumed for this subcatalog is not very far from the corner magnitude  $m_c = 5.87 \pm 0.17$  that Bird & Kagan (2004) inferred for normal-faulting earthquakes on OSR steps. Therefore, most of the scalar moments added in this sum are approximately the same size, at least within one order-of-magnitude. This parallelism between earthquake counts and moment sums suggests that the primary factor varying with spreading rate is the mean coupled thickness of seismogenic

lithosphere  $\langle cz \rangle$ . Bird & Liu (2007) estimated that it declines from a peak value of about 1.5 km at very low spreading rates, and that the velocity scale for this quasi-exponential reduction is about 19 mm/a. The global mean  $\langle cz \rangle$  for normal-faulting earthquakes on all OSRs is only 0.13 km (Bird & Kagan, 2004). These very small thicknesses probably are proportional to the thicknesses of frozen lids over the magma (and/or partial-melt) chambers that underlie the centers of spreading ridges and limit their vertically-integrated strengths to very low values.

#### More earthquakes (per unit of slip) at high velocities: Subduction Zones and Continental Convergent Boundaries

A Subduction zone (SUB) in the PB2002 classification of Bird (2003) is a plate boundary with convergent velocity and associated Quaternary volcano(s) about 200 km away, and/or a Wadati-Benioff zone of intermediate-depth seismicity. “Oceanic” versus “continental” lithosphere is not a criterion because many subduction zones occur at a boundary between the two, or have intermediate character. Our sample of the seismicity associated with subduction is defined as shallow ( $\leq 70$  km depth) but includes earthquakes of all mechanisms, whether from low-angle thrusting on the intraplate shear zone, plate bending, or strike-slip in oblique subduction settings with partitioning. As explained in Bird & Kagan (2004), the primary criterion for associating a shallow earthquake with a subduction zone is that it occurs within (or close to) a “lane” which is projected from the plate-boundary step into both neighboring plates along the azimuth of their relative velocity. The sample of seismicity (outside orogens) from the complete part of the CMT catalog ( $M_t = 3.47 \times 10^{17}$  N m) is therefore very large: 2057 earthquakes, of which 1526.3 are estimated to be independent.

The cumulative independent earthquake curve in Figure 6 shows a curvature in the opposite sense to that of OSRs: it is concave-upward, indicating that earthquake production per

unit of slip, or per unit of relative velocity, is greater at higher velocities. Slower subduction at  $\leq 66$  mm/a (which produces the first 35% of cumulative tectonic moment rate under the null hypothesis) produces only the first 20% of cumulative independent subduction earthquakes. Therefore, mean earthquake productivity in the upper 65% of cumulative tectonic moment rate (according to the null hypothesis) is about twice as great. The K-S statistic for departure of this curve from the diagonal is 0.1514 and the C-v-M statistic is 0.0897; both lie far outside the range that we found in 10,000 Monte-Carlo simulations of the null hypothesis (for this subcatalog size and plate boundary geometry), so both have probabilities of exceedance  $P \ll 0.0001$  under the null hypothesis, which is rejected.

Continental Convergent Boundaries (CCBs) in the PB2002 classification of Bird (2003) are convergent plate boundaries in continental lithosphere (defined above) which do not have either a parallel arc of Quaternary volcanoes or a Wadati-Benioff zone of intermediate-depth seismicity. As in all sections of this paper, we exclude seismicity in any of the 13 orogens of PB2002, so the Himalayas and some parts of the Andes are not part of this sample (see Liu & Bird, 2008). The earthquake count (above  $M_t = 3.47 \times 10^{17}$  N m) is therefore modest: 300 events, of which 233.7 are estimated to be independent. The cumulative independent earthquake count for CCBs is seen in **Figure 7**, which has a very similar concave-upward form to that for subduction zones in Figure 6. The kink in the curve, at which seismic productivity increases, is at relative tectonic moment rate 50% and relative seismicity 30%, so the change in productivity is again by about a factor of two. (However, the relative plate velocity corresponding to this kink is 24 mm/a, which is slower than the 67 mm/a at which productivity of SUBs appears to change.) There is a suggestion that the slowest-slipping ( $< 10$  mm/a) and fastest-slipping ( $> 80$  mm/a) CCB boundaries may come closer to the linear behavior of the null hypothesis than those

with intermediate velocities. The K-S statistic for departure of this curve from the diagonal is 0.195 and the C-v-M statistic is 0.085; both lie outside the range that we found in 10,000 Monte-Carlo simulations of the null hypothesis (for this subcatalog size and plate boundary geometry), so both have probabilities of exceedance  $P < 0.0001$  under the null hypothesis, which is rejected.

SUB and CCB plate boundary classes both produce more earthquakes per unit of intraplate slip when the plate convergence velocity is high. This unexpected result is the principal new discovery of our study. We therefore expand this discussion to cover two obvious questions: (1) Why was this nonlinearity not found in the previous investigation by Kreemer *et al.* (2002); and (2) what physical mechanisms might explain this velocity-dependence?

#### Comparison to results of Kreemer *et al.* (2002)

Kreemer *et al.* (2002) conducted a similar study, resulting in four graphs (their Figures 1A-D) similar in format to our Figures 1-7. Their abscissas were cumulative tectonic moment rates in N m/yr, based on assumed values of (what we call) coupled thickness  $\langle cz \rangle$  which were constant within each plot; except for the distinction between dimensional and nondimensional numbers, these abscissas are comparable in principle. Their ordinates were labeled as cumulative seismic moment (as a fraction of total seismic moment), but it was explained in their text that most of the numbers displayed were “predicted moment rates” based on earthquake counts, so these ordinates are also comparable in principle. They did not compute statistical significances of departures from linearity. Their “Subduction Zones” province (their Fig. 1A) shows a linear relation, quite different from the concave-upward curvature in our Figure 6 (SUBs). Their “Continental” province (their Fig. 1B) shows higher earthquake production (15~20% of total) in the slowest decile of model tectonic moment rate, with a linear relation thereafter; thus the sense of curvature near the origin is opposite from that seen in our Figure 7

(CCBs), but the subsequent linearity is similar to our Figures 1 (CTFs) and 2 (CRBs). Their “Ridges & Transforms” province (their Fig. 1C) shows a convex-upward curve, not as strongly curved as our Figure 5 (OSRs), but more strongly curved than our Figure 3 (OTFs); considered as an average of the two it appears consistent. Their “Diffuse Oceanic” province (their Fig. 1D) shows a complex shape quite similar to that of our Figure 4 (OCBs).

Thus, the primary discrepancy concerns the linearity, or curvature, of the relationship in subduction zones. (There is also a more complex issue concerning behavior of slow-deforming continental lithosphere.) The list of potential causes for this discrepancy includes at least 7 differences between our studies, which may affect abscissas, ordinates, or both: (i) The kinematic model of Kreemer *et al.* (2002) was the Global Strain Rate Map solution later published by Kreemer *et al.* (2003), whereas ours is rigid-plate model PB2002 by Bird (2003). (ii) They included both simple and complex plate boundaries, whereas our study is restricted to simple plate boundaries. (iii) They computed tectonic moment rates from strain-rates (including elastic components), whereas we compute them from long-term-average fault slip rates. Varying assumed widths of the plate-boundary zones of straining in the GSRM model affect the ordering of regions along their abscissas, whereas ordering of regions along our abscissas is strictly by relative plate velocity. (iv) They divided tectonics and seismicity into 4 “deformation regimes” whereas PB2002 and this study recognize 7 “classes of plate boundary.” (v) They assigned earthquakes to deformation regime subcatalogs according to a colored map (their Plate 2), whereas we assign each earthquake to a particular plate boundary step of model PB2002 based on location, depth, focal mechanism, and a prior model of the seismicity of that step, and then choose the seismic subcatalog based on the class of that step. (vi) They used years 1977-2000 and depths 0-40 km from the CMT catalog, whereas we use years 1982-2007 and depths 0-70

km. (They also analyzed earthquakes from the PDE catalog 1968-1997, which we do not.) (vii) Kreemer *et al.* (2002) did not decluster their catalog, or weight earthquakes by their independence as we do, before accumulating earthquake counts.

Of these differences, the one most likely to be decisive is (v), the assignment of earthquakes to subcatalogs. Kreemer *et al.* (2002) did not include all the “Subduction zones (SUBs)” of model PB2002 (Bird, 2003) in their “Subduction zone deformation regime.” The ones that we consider to have been omitted are highlighted in our **Figure 8**: Aegean-Cyprus, west & north Sulawesi, north Kamchatka, Puysegur & Hikurangi, Cascadia, Maracaibo, south Antilles, and South Shetland subduction zones. As all of these omitted zones have relatively slow rates of convergence and modest seismicity, it may be reasonable to say that Figure 1A of Kreemer *et al.* (2002) omits most cases of slow subduction, and corresponds very roughly to the straight-line portion of our Figure 6 which begins at relative cumulative tectonic moment rate of 0.35.

#### Physical mechanisms for velocity-dependence in subduction zones

These exploratory comments focus mainly on the subduction process. However, to the extent that some Continental Convergent Boundaries are dominated by a single master thrust fault which carries young water-saturated sediments down into the seismogenic depth range of the fault, the physics controlling seismicity of CCBs may be similar to those of SUBs. We briefly consider three ways in which subduction velocity might affect earthquake production: through thermal structure, through the viscous limit on strength, or through pore pressure. The first linkage receives the fullest development, because quantitative models are possible.

## Thermal structure:

One way that subduction velocity might control seismicity is by varying the thermal structure of the forearc where the great intraplate thrust events occur. Specifically, the down-dip limit of the seismogenic portion of the intraplate thrust fault might be controlled by a critical temperature, and this temperature might be advected deeper by faster subduction. Subduction zones have low heat-flow in their forearcs due to heat advection by the downward component of subducting plate motion beneath them. This is easy to model in a vertical cross-section plane. Volcanic arcs of subduction zones have elevated heat-flow due to heat advection by upward flow of magma and volatiles. This is harder to model, both because it is a multiphase 3-D time-dependent process, and because we lack basic information on the sizes of these fluxes and their mode(s) of transport. Still, the lateral flux of heat into the forearc can be approximated by fixing a reasonable mean geotherm in the volcanic arc, and using this as the lateral boundary condition. Such a model can provide insight on how thermal structure of the seismogenic forearc is likely to vary with subduction rate.

For exploratory purposes, we compute a set of time-dependent 2-D F-D models of a simplified subduction forearc, using the alternating-direction-implicit algorithm (Press *et al.*, 1986, p. 660-667) to represent diffusion of heat, and using simple translation of temperatures across the grid to represent motion of the subducting plate. In these models, the subducting plate descends by 80 km over a horizontal distance of 220 km at a constant dip angle of  $20^\circ$ . (The upper surface of our model domain is the seafloor, which is an isothermal surface at 0 C. Typically this has a mean trenchward slope of about  $2.6^\circ$  across the forearc. If our model is rotated to reflect this, then the dip of our subduction shear zone becomes  $17.4^\circ$ , as in **Figure 9**.) Translation of the subducting plate is always by exactly one grid row and one grid column per

time step, preventing unwanted numerical diffusion in the advection steps. The intraplate shear zone is centered on a diagonal of F-D grid points (where the translation operation is scaled down by 50%), and shear-strain heating is applied only to these points. Heat-flow is fixed at 45 mW/m<sup>2</sup> where the subducting plate enters at one side of the grid, and 90 mW/m<sup>2</sup> in the volcanic arc on the other side. The geotherm under the arc is limited by melting to  $\leq 1200^{\circ}\text{C}$ . Thermal conductivity is uniform at 3 W/m/°K, thermal diffusivity is uniform at  $1 \times 10^{-6}$  m<sup>2</sup>/s, and radioactivity is neglected. Shear-strain heating on the intraplate thrust fault is determined by a uniform shear traction of only 10 MPa (Bird, 1978; Peacock, 1992; Hyndman & Wang, 1993; Geist, 1996; Bird *et al.*, 2008). All models are run for 100 m.y. and are very close to steady-state at the end.

This set of models (*e.g.*, **Figure 9**) shows very modest variations of temperature with subduction velocity, especially among the high-velocity models. This is because the first-order thermal balance is between cooling by downward advection and heating by deformation in the intraplate shear zone, and both of these effects are proportional to velocity (van den Beukel & Wortel, 1987; Peacock, 1992). A second-order dependence of shear zone temperatures appears because slower subduction allows diffusive averaging of temperatures to reach deeper into the subducting plate, where initial temperatures were higher. Thus, the shear zone is slightly warmer at low subduction velocities.

We refer to previous studies of the aftershock zones and stress-drop patches of great subduction zone earthquakes to determine the typical location of the stick-slip portion of the shear zone. In the 4 subduction zones which Oleskevich *et al.* (1999) studied (along 12 profiles), the mean width of the seismogenic patch was 104 km at a mean subduction velocity of 55 mm/a. Studies by Tichelaar & Ruff (1993) and by Oleskevich *et al.* (1999) agreed in finding that the

mean depth to the lower limit of the seismogenic patch is 40 km. Based on these constraints, we select model shear-zone temperatures of 0 to 150 C as defining the limits of the model seismogenic patch. Our upper temperature limit is lower than model temperature limits for frictional sliding in subduction zones inferred by Tichelaar & Ruff (1993) and by Oleskevich *et al.* (1999), primarily because we assume lower shear stresses, but it should serve for comparisons in which we try to extract the effect of subduction velocity with all other factors held constant.

In **Figure 10** we show the variations in this model depth (below the seafloor) to the lower limit of the seismogenic patch in the subduction shear zone, assuming it is controlled by a fixed critical temperature. We see that it varies by a factor-of-two, from 19 km to 41 km, as subduction velocity is increased from 5 to 240 mm/a. Most of the change takes place in the velocity range below 70 mm/a, at which the depth is 39 km.

Although these depths to the 150 C isotherm are relative to the sea floor, they occur in a part of the forearc (55 to 110 km inland from the trench) which is typically occupied by the outer part of a forearc basin, with shallow seas and/or low-lying land. Therefore, these depths are almost the same as predicted depths with respect to sea level. If we subtract the depth (with respect to sea level) at which the seismogenic patch begins, the result will be the “seismogenic lithosphere thickness”  $z$  as defined by Bird & Kagan (2004). In **Figure 11**, we display  $z$  as a function of subduction velocity when the seismogenic patch begins 12.4 km below sea level. (This particular depth is slightly different from the 14-km depth that Bird & Kagan (2004) estimated based on data in Oleskevich *et al.* (1999), but it has the virtue of preserving the global-mean  $z$  of 26 km for subduction zones which Bird & Kagan used in their Table 5 to estimate seismic coupling.)

These variations of  $z$  in Figure 11 can be used to predict model variations in seismic moment rate (of intraplate shear-zone earthquakes) with subduction velocity, if we assume that the seismic coupling coefficient ( $c$  of Bird & Kagan, 2004) is independent of velocity. (Possible velocity-variations of  $c$  will be discussed in the next two sections.) Variations in  $z$  are also relevant to predicted variations in the corner moment ( $M_c$ ) and associated corner magnitude ( $m_c$ ) of the largest expected earthquakes, as defined by Bird & Kagan (2004). For modeling corner events, it is probably best to assume local  $c = 1$  and also to assume a mean dip of the seismogenic patch ( $\theta$  of Bird & Kagan, 2004) which is not velocity-dependent. Then, we would expect scaling of either  $M_c \sim z^2$  or  $M_c \sim z^3$ . The first factor of  $z$  comes from the increased width of the rupture patch (at constant dip, with perfect coupling). The second factor of  $z$  comes from the increase in mean slip (for fixed stress-drop) as the minimum dimension of the rupture patch increases. A third factor of  $z$  might appear if the rupture shapes of subduction corner events are self-similar as velocity changes; that is, if ruptures in thinner seismogenic lithosphere are expected to propagate shorter distances along strike. In Figure 12, we display model variations in corner magnitude  $m_c$  that would be expected based on either scaling. The curves are pinned at the best-estimate corner magnitude of 9.58 from Bird & Kagan (2004) when subduction velocity is 77 mm/a (as it was at the site of the critical 1960.05.22  $m9.64$  Chilean earthquake). The predicted variations are modest:  $m_c$  does not drop below 9.0 until velocity drops below 16 mm/a ( $M_c \sim z^3$  scaling) or 9 mm/a ( $M_c \sim z^2$  scaling). Considering the low seismicity of such slow subduction zones, it might take as much as  $10^3$  to  $10^4$  years to conduct a meaningful test of this prediction (although it could be disproven any day). At the lowest subduction velocities, this scaling is also expected to break down because other types of

earthquakes will become larger than the largest events on the intraplate shear zone. Plate-bending earthquakes can be as large as  $m8.39$  (1933.03.02 Sanriku earthquake offshore Japan), and these take place in a thermal environment that is entirely determined by lithospheric age, independent of the rate of subduction. As seen in Figure 12, bending events are expected to dominate in determining the corner magnitude for subduction rates less than 5 mm/a ( $M_c \sim z^3$  scaling) or  $\sim 2$  mm/a ( $M_c \sim z^2$  scaling).

Finally, we are able to predict the thermal part of the velocity-dependence of earthquake rates in subduction zones. Increasing subduction rate will increase the seismogenic lithosphere thickness (tending to raise earthquake productivity), but it will also increase the corner magnitude (tending to lower earthquake productivity). We make a number of simplifying assumptions: (i) constant mean coupling  $\langle c \rangle (\cong 0.69, \text{Bird \& Kagan, 2004})$ , (ii) constant spectral slope  $\beta = 0.64$  (Kagan, 1999; Bird & Kagan, 2004), (iii) constant dip of the seismogenic part of the intraplate shear zone, and (iv) orthogonal subduction, so subduction velocity equals relative plate velocity. In this case, earthquake productivity  $P^*$  (shallow earthquake count above threshold  $m_t = 5.66$ , per unit of catalog duration, per unit length of trench, per unit of relative plate velocity) should vary with relative plate velocity  $v$  as:

$$\frac{P^*(v)}{\langle P^* \rangle} = \langle S \rangle \frac{z(v)/\langle z \rangle}{\left( M_c^{1-\beta}(v) M_t^\beta - M_t \right) / \left\langle \left( M_c^{1-\beta} M_t^\beta - M_t \right) \right\rangle} + (1 - \langle S \rangle) \quad (3)$$

where  $\langle \rangle$  indicates a global average over subduction zones (weighted by model tectonic moment rate), and  $\langle S \rangle$  is the mean fraction of shallow subduction-zone earthquakes with  $m > m_t$  which are produced in the intraplate shear zone. Based on a global compilation of shallow CMT focal mechanisms in subduction zones (1977.01.01-2002.09.30), we estimate

$\langle S \rangle = 0.62$  (**Figure 13**). This leads to predicted variations in normalized productivity which are displayed in **Figure 14**.

These predicted variations are very modest: no more than 20%. Furthermore, the sense of the predicted variation depends on which scaling of corner magnitude against seismogenic depth is selected. Clearly, thermal effects alone are unlikely to provide an explanation for the factor-of-two variations in actual subduction-zone earthquake productivity that we saw in Figure 6, or variations of productivity of continental convergence zones seen in Figure 7.

### **Viscous limits on strength:**

One of the subduction zones in our “slow” category ( $v \leq 66$  mm/a) is the Aegean (or Hellenic)-Cyprus subduction zone, which presently consumes Mediterranean seafloor of the Africa plate at rates of at least 38 mm/a (McClusky *et al.*, 2000; Bird, 2003; the long-term rate may be faster if there has been elastic strain accumulation during the geodetic epoch). In the Messinian salinity crisis at  $\sim 6$  Ma the Mediterranean Sea dried up, leaving much of this seafloor coated with sulfate evaporites and/or halite in the deepest sub-basins (Hsü, 1972). In **Figure 15**, we show how far this evaporite material might have been underplated in the various subduction zones of the Mediterranean basin, assuming in each case that at least some of the evaporite moved with the subducting plate at rates given by the neotectonic model PB2002 (Bird, 2003). Evaporites could potentially underlie the entire forearc of the Aegean subduction zone, providing a low-viscosity layer that might have the effect of suppressing earthquakes on the intraplate shear zone. The reduction in overall earthquake productivity could be by a factor no smaller than  $1 - \langle S \rangle \cong 0.38$ , since plate-bending earthquakes and upper-plate earthquakes would not be affected. Some support for this hypothesis comes from the study of Shaw *et al.* (2008), who found that the great tsunamigenic earthquake of AD 365 (in or near Crete) occurred within the

upper plate of the subduction zone, and that such great earthquakes are an order-of-magnitude more rare in the historic record than expected from the model tectonic moment rate. (However, the interplate shear zone is not completely aseismic, as shown by focal mechanisms described by Taymaz *et al.*, 1990.)

Underplating by evaporites may also affect the seismicity of other subduction zones in the Mediterranean basin, such as the Calabrian and the North Sicilian (Figure 15), although the extent of underplating is probably no more than  $6 \text{ Ma} \times 8 \text{ mm/a} = 48 \text{ km}$  downdip. The latter two zones were included in the “Alps” orogen of the PB2002 model (because their convergence rates are uncertain and potentially less than AF-EU rates), so their earthquake productivities do not affect our test for linearity (Figure 6). The Aegean-Cyprus zone is included, but its contribution to model tectonic moment rate is only 1.7% of the global total for all subduction zones, and only 4.9% of the total for “slow” subduction zones. Therefore, even the most generous estimate of the evaporite effect cannot explain more than a small fraction (~4%) of the velocity-dependence of subduction zones seen in Figure 6.

However, there are more common types of seafloor sediment which might be weak enough to suppress coupling and seismicity of interplate shear zones. Candidates include montmorillonite-rich layers of altered volcanic ash (Vrolijk, 1990; Deng & Underwood, 2001), siliceous radiolarian and diatomaceous oozes, and calcareous foraminiferal oozes. (Calcareous oozes are generally soluble in deep ocean waters, but they can be preserved by blanketing sediments, as evaporites have been.) Since the rheologic laws for these materials are not well-known, it is conceivable that their effective viscosities ( $\mu$ ) might be low enough to allow relative plate motion to occur by a viscous process, with shear stresses suppressed below the level necessary for frictional sliding in earthquakes. Effective viscosities  $\mu$  would have to be:

$$\mu < \frac{\sigma_s t}{v} \quad (4)$$

where  $\sigma_s$  is the shear stress on the interplate shear zone required for earthquakes, and  $t$  is the thickness of the viscous sediment layer after subduction. (In a steady-state viscous subduction model, this should be about twice the thickness of undisturbed pelagic sediments on the subducting plate.) If we estimate  $\sigma_s$  by the typical level of shear traction on interplate shear zones as 10 MPa (Bird, 1978; Geist, 1996; Bird *et al.*, 2008), and a typical thickness of viscous subducted sediment is  $2 \times 500 \text{ m} = 1 \text{ km}$ , then  $\mu < 1 \times 10^{19} \text{ Pa s}$  for seismicity suppression at  $v = 30 \text{ mm/a}$ , or  $\mu < 3 \times 10^{18} \text{ Pa s}$  for seismicity suppression at  $v = 90 \text{ mm/a}$ . The velocity-dependence in (4) means that it would not be necessary to assume any spatial correlation between weak sediment and slow subduction; the inherent velocity-dependence of the viscous mechanism competing with frictional sliding could explain the bend in Figure 6. In theory, all that would be required is universal subduction of a 500-m layer of pelagic sediment with effective viscosity  $2 \times 10^{18} \text{ Pa s}$ . If this caused  $\sim 75\%$ -reduction in intraplate shear zone seismic productivity, the remainder would be about 1/3 of “normal” (*i.e.*, fast-subduction) productivity, and the constant plate-bending contribution could supply the rest of the slow-subduction earthquakes we observe.

Of course, there are several important factors that would complicate this hypothesis. Pelagic sediment is not uniform in thickness or in composition, but varies with (paleo-)latitude, primary productivity, seafloor depth, and windborne dust supply. (The overlay of trench turbidities occurring in many subduction zones is probably irrelevant, as pelagic sediments are probably weaker than clastic turbidites.) It would be surprising if all pelagic seafloor sediment could be described by a single effective viscosity. Second, many rocks deform by power-law

mechanisms (*e.g.*, dislocation creep, grain-size-dependent solution transfer) which would make the velocity-dependence of viscous shear stress less than linear (**Figure 16**). Third, many seamounts have relief exceeding 1 km, and these would bridge the viscous layer to create asperities.

### **Velocity-dependent pore pressures:**

It is often suggested that the low shear stresses in the seismogenic portions of subduction shear zones (~10 MPa, Bird, 1978; Geist, 1996; Bird *et al.*, 2008) are regulated by super-hydrostatic pore pressures (*e.g.*, Saffer, 2003; Gomberg *et al.*, 2008; Gerya *et al.*, 2008), rather than by very low coefficients of internal friction. Pelagic sediment subducted at the trench has higher porosity and water content than deformed equivalents seen in exhumed subduction mélanges like the Franciscan Formation of California, which means that there is relative flow between the sediments (traveling faster down-dip) and the pore waters (traveling more slowly). This relative flow is driven by super-hydrostatic gradients of pore pressure in the downdip direction, which are in turn regulated by the nonlinear dependence of permeability on effective confining pressure. This qualitative model is supported by observations of seafloor mud volcanoes in forearcs, and by the elevated pore pressures observed by ODP Leg 19 (1995).

Unfortunately this popular model has not yet been reduced to a quantitative form with predictive capabilities (Langseth & Moore, 1990). A quantitative form would need to include, at least: nonlinear and temperature-dependent relations between effective pressure and compaction rate, nonlinear relations between grain-size and effective pressure and permeability, mineral stability diagrams predicting “water” (*i.e.*, proton) storage in crystallographic sites; rheologic laws capable of predicting the evolution of grain-size, a thermal model, and some approximation of pore pressure regulation and water transport by dike propagation in an anisotropic stress field.

Despite these complications, it is clear that faster subduction should result in pore pressures further from hydrostatic and closer to lithostatic. This would reduce the shear stress necessary for frictional sliding, making it more likely. If the shear stress needed for earthquakes is a declining function of subduction rate,  $\sigma_s(v)$ , this process would interact constructively with the velocity-dependence of viscous stress to suppress seismicity below a critical subduction rate (Figure 16).

### Discussion

This study examines the consistency of the CMT catalog data with a null hypothesis of uniform earthquake productivity (shallow independent earthquake count above threshold  $m_t$ , per unit of catalog duration, per unit of plate boundary length, per unit of relative plate velocity) within each of the 7 classes of plate boundary in the PB2002 model. Results from Continental Transform Faults (CTFs) and Continental Rift Boundaries (CRBs) are consistent with the null hypothesis. Oceanic Transform Faults (OTFs) and Oceanic Convergent Boundaries (OCBs) show marginally significant nonlinearity, but these weak nonlinearities could be artifacts of an inhomogeneous subcatalog in the first case, and earthquake or plate boundary mis-classification in the second. Oceanic Spreading Ridges (OSRs) are strongly nonlinear, with greater earthquake productivity and greater seismicity at lower spreading rates; this result has been obtained many times before by other authors using other methods of analysis.

Our most interesting new result is the nonlinearity of Subduction zones (SUBs) and Continental Convergent Boundaries (CCBs), both of which display lower earthquake productivity, by about a factor-of-two, below a critical relative plate velocity. For SUBs this velocity is  $\sim 66$  mm/a, while for CCBs it is  $\sim 24$  mm/a. We discussed three physical mechanisms for such velocity-dependence of subduction, and found that variations in thermal structure are

not likely to play a major role (at least, under the simple assumptions of our thermal model). On the other hand, viscosity of subducted sediments and velocity-dependent pore pressures in SUBs (and possibly CCBs) both predict the right sense of nonlinearity, and could act either independently or constructively to produce this result.

Because only the thermal mechanism for nonlinearity has been developed quantitatively, this is the only model for which we can derive predictions of velocity-dependent variations in corner magnitude  $m_c$ , which we find to be modest. For the other two mechanisms the effect on corner magnitude remains unclear. None of the mechanisms we examined led to predictions of asymptotic spectral slope  $\beta$  of the tapered Gutenberg-Richter frequency/magnitude relation; however, this may not be important as there are signs that constant  $\beta$  may be a universal property of shallow seismicity (Bird & Kagan, 2004). Unfortunately, we cannot presently predict the velocity-dependent(?) behavior of these other two parameters used in forecasting rates of large, destructive earthquakes in these two types of plate boundaries. Until our knowledge improves, it may be reasonable to forecast the long-term seismicity of SUBs and CCBs by simply using the global-average values of  $m_c$  and  $\beta$  obtained by Bird & Kagan (2004) for these plate boundary classes. The lower earthquake productivity of slowly-converging boundaries can be introduced by reducing their coupled seismogenic lithosphere thickness  $\langle cz \rangle$  at relative plate velocities below their critical velocities, while slightly elevating it for higher velocities and thus preserving the empirical global mean. The subduction zones for which  $\langle cz \rangle$  should be reduced are those shown with broad lines in Figure 8, plus their lateral extensions into adjacent orogens.

## **Data and Resources**

For each of the 7 classes of plate boundary (generically *XXX*, where *XXX* = CCB, CRB, CTF, OCB, OSR, OTF, SUB, as defined above) we provide 2 computer files:

CMT\_PB2002\_XXX\_pure.eqc is the corresponding subcatalog (above threshold) for the non-orogen parts of Earth's surface, as defined by Bird (2003). Each subcatalog is in the .eqc file format defined in the electronic attachments to Bird & Kagan (2004). The Fortran 90 code (EQ\_classification\_II.f90) used to divide the CMT catalog into 7 subcatalogs was previously published by Bird & Kagan (2004).

PB2002\_XXX\_pure\_independent\_CMT.txt is a tab-delimited headerless ASCII table listing plate boundary steps of one class in order by relative plate velocity, and showing the summations of model tectonic moment rate, independent earthquake count, and independent seismic moment sum that we display in Figures 1-7. To access these files, and to read definitions of the columns in headerless ASCII tables, please refer to the **electronic supplement**.

## **Acknowledgments**

This research was supported by the National Science Foundation (NSF) under grant number EAR-0711515. The views and conclusions contained in this document are those of the authors and should not be interpreted as necessarily representing the official policies, either expressed or implied, of the U.S. Government. This research was also partly supported by the Southern California Earthquake Center (SCEC). SCEC is funded by NSF Cooperative Agreement EAR-0529922 and USGS Cooperative Agreement 07HQAG0008. The SCEC contribution number for this paper is 1264.

## References Cited

- Bennett, R. A., S. Hreinsdóttir, G. Buble, T. Bašić, Ž. Bačić, M. Marjanović, G. Casale, A. Gendaszek, and D. Cowan (2008). Eocene to present subduction of southern Adria mantle lithosphere beneath the Dinarides, *Geology* **36**(1), 3-6, doi 10.1130/G24136A.1.
- Bird, P. (1978). Stress and temperature in subduction shear zones: Tonga and Mariana, *Geophys. J. R. Astron. Soc.* **55**, 411-434.
- Bird, P. (2003). An updated digital model of plate boundaries, *Geochemistry Geophysics Geosystems* **4**(3), 1027, doi10.1029/2001GC000252.
- Bird, P., and Z. Liu (2007). Seismic hazard inferred from tectonics: California, *Seismol. Res. Lett.* **78**(1), 37-48.
- Bird, P., and Y. Y. Kagan (2004). Plate-tectonic analysis of shallow seismicity: Apparent boundary width, beta, corner magnitude, coupled lithosphere thickness, and coupling in seven tectonic settings, *Bull. Seismol. Soc. Am.* **94**(6), 2380-2399, plus electronic supplement.
- Bird, P., Y. Y. Kagan, and D. D. Jackson (2002). Plate tectonics and earthquake potential of spreading ridges and oceanic transform faults, *Plate Boundary Zones, Geodynamics Series* **30**, S. Stein and J. T. Freymueller (Editors), American Geophysical Union, Washington, DC, 203-218.
- Bird, P., Z. Liu, and W. K. Rucker (2008). Stresses that drive the plates from below: Definitions, computational path, model optimization, and error analysis, *J. Geophys. Res.* **113**(B11), B11406, doi10.1029/2007JB005460, plus digital appendices.
- Brune, J. N. (1968). Seismic moment, seismicity, and rate of slip along major fault zones, *J. Geophys. Res.*, **73**, 777-784.

- DeMets, C., R. G. Gordon, and D. F. Argus (2009) Geologically current plate motions, *Geophys. J. Int.*, in press as of 2009.07.
- Deng, X., and M. B. Underwood (2001). Abundance of smectite and the location of a plate-boundary fault, Barbados accretionary prism, *Geol. Soc. Am. Bull.* **113**(4), 495-507.
- Ekström, G., A. M. Dziewonski, N. N. Maternovskaya and M. Nettles (2005). Global seismicity of 2003: Centroid-moment-tensor solutions for 1087 earthquakes, *Phys. Earth Planet. Inter.* **148**(2-4), 327-351.
- Frohlich, C., and K. D. Apperson (1992). Earthquake focal mechanisms, moment tensors, and the consistency of seismic activity near plate boundaries, *Tectonophysics* **11**, 279-296.
- Geist, E. L. (1996). Relationship between the present-day stress field and plate boundary forces in the Pacific Northwest, *Geophys. Res. Lett.* **23**(23), 3381-3384.
- Gerya, T., J. A. D. Connolly, and D. A. Yuen (2008). Why is terrestrial subduction one-sided?, *Geology* **36**(1), 43-46, doi 10.1130/G24060A.1.
- Gomberg, J., A. M. Trehu, E. Roeloffs, and H. Dragert (2008). Understanding slow slip, tremor, and quakes, *Eos Trans. AGU* **89**(34), 315.
- Hanks, T. C., and H. Kanamori (1979). A moment magnitude scale, *J. Geophys. Res.* **84**, 2348-2350.
- Hsü, K. J. (1972). When the Mediterranean dried up, *Sci. Am.* **227**(6), 26-36, Dec. 1972.
- Hyndman, R. D., and K. Wang (1993). Thermal constraints on the zone for major thrust earthquake failure: The Cascadia subduction zone, *J. Geophys. Res.*, **98**, 2039-2060.
- Jackson, D. D., and Y. Y. Kagan (1999). Testable earthquake forecasts for 1999, *Seism. Res. Lett.* **70**, 393-403.

- Kagan, Y. Y. (1991). Likelihood analysis of earthquake catalogs, *Geophys. J. Int.* **106**(1), 135-148.
- Kagan, Y. Y. (2003). Accuracy of modern global earthquake catalogs, *Phys. Earth. Planet. Int.* **135**(2-3), 173-209, doi 10.1016/S0031-9201(02)00214-5.
- Kagan, Y. Y., and D. D. Jackson (2000). Probabilistic forecasting of earthquakes, *Geophys. J. Int.* **149**, 438-453.
- Kagan, Y. Y., P. Bird, and D. D. Jackson (2009). Earthquake patterns in diverse tectonic zones of the globe, in press at *PAGEOPH* as of 2009.03.23. Final manuscript version available at [http://moho.ess.ucla.edu/~kagan/globe\\_rev.pdf](http://moho.ess.ucla.edu/~kagan/globe_rev.pdf)
- Kagan, Y. Y., and L. Knopoff (1976). Statistical search for non-random features of the seismicity of strong earthquakes, *Phys. Earth Planet. Inter.* **12**, 291-318.
- Kanamori, H. (1977). Seismic and aseismic slip along subduction zones and their tectonic implications, in M. Talwani & W. C. Pitman III (editors), *Island Arcs, Deep Sea Trenches, and Back-Arc Basin, Maurice Ewing Series*, **1**, 163-174.
- Kostrov, B. V. (1974). Seismic moment and energy of earthquakes, and seismic flow of rocks, *Izv. Acad. Nauk. SSR Phys. Solid Earth*, **1**, 23-44.
- Kreemer, C., W. E. Holt, and A. J. Haines (2002). The global moment rate distribution within plate boundary zones, in S. Stein & J. T. Freymueller (editors), *Plate Boundary Zones, Geodynamics Series* **30**, 173-190.
- Kreemer, C., W. E. Holt, and A. J. Haines (2003). An integrated global model of present-day plate motions and plate boundary deformation, *Geophys. J. Int.* **154**, 8-34.
- Langseth, M. G., and J. C. Moore (1990) Fluids in accretionary prisms, *Eos Trans. AGU* **71**(5), 235 & 245-246.

- Liu, Z., and P. Bird (2008). Kinematic modelling of neotectonics in the Persia-Tibet-Burma orogen, *Geophys. J. Int.* **172**(2), 779-797; doi10.1111/j.1365-246X.2007.03640.x, + 3 digital file appendices.
- McCaffrey, R. (1997a). Statistical significance of the seismic coupling coefficient, *Bull. Seismol. Soc. Am.*, **87**, 1069-1073.
- McCaffrey, R. (1997b). Influences of recurrence times and fault zone temperatures on the age-rate dependence of subduction zone seismicity, *J. Geophys. Res.*, **102**, 22839-22854.
- McClusky, S., and 27 others (2000). Global Positioning System constraints on plate kinematics and dynamics in the eastern Mediterranean and Caucasus, *J. Geophys. Res.* **105**, 5695–5719.
- ODP Leg 16 Shipboard Drilling Party (1995). Seismic images and drilling tell a story of fluids in a plate-boundary fault, *Eos Trans. AGU* **76**(18), 185-186.
- Oleskevich, D. A., R. D. Hyndman, and K. Wang (1999). The updip and downdip limits to great subduction earthquakes: Thermal and structural models of Cascadia, south Alaska, SW Japan, and Chile, *J. Geophys. Res.* **104**, 14965-14991.
- Pacheco, J. F., L. R. Sykes, and C. H. Scholz (1993). Nature of seismic coupling along simple plate boundaries of the subduction type, *J. Geophys. Res.*, **98**, 14133-14159.
- Peacock, S. M. (1992). Blueschist-facies metamorphism, shear heating, and P-T-t paths in subduction shear zones, *J. Geophys. Res.*, **97**, 17693-17707.
- Press, W. H., B. P. Flannery, S. A. Teukolsky, and W. T. Vetterling (1986). *Numerical Recipes: The Art of Scientific Computing*, Cambridge University Press, 818 pages.

- Rosenbaum, G., M. Gasparon, F. P. Lucente, A. Peccerillo, and M. S. Miller (2008). Kinematics of slab tear faults during subduction segmentation and implications for Italian magmatism, *Tectonics* **27**(2), TC2008, doi 10.1029/2007TC002143.
- Ruff, L., and H. Kanamori (1980). Seismicity and the subduction process, *Phys. Earth Planet. Int.*, **23**, 240-253.
- Ruff, L., and H. Kanamori (1983). Seismic coupling and uncoupling at subduction zones, *Tectonophysics*, **99**, 99-117.
- Saffer, D. M. (2003). Pore pressure development and progressive dewatering in underthrust sediments at the Costa Rican subduction margin: Comparison with northern Barbados and Nankai, *J. Geophys. Res.* **108**(B5), 2261, doi 10.1029/2002JB001787.
- Shaw, B., N. N. Ambraseys, P. C. England, M. A. Floyd, G. J. Gorman, T. F. G. Higham, J. A. Jackson, J.-M. Nocquet, C. C. Pain, and M. D. Piggott (2008). Eastern Mediterranean tectonics and tsunami hazard inferred from the AD 365 earthquake, *Nature Geoscience* **1**, 268 – 276, doi10.1038/ngeo151.
- Simkin, T., and L. Siebert (1995). *Volcanoes of the World*, Smithsonian Inst., Washington, D. C..
- Sobolev, P. O., and D. V. Rundquist (1999). Seismicity of oceanic and continental rifts—a geodynamic approach, *Phys. Earth Planet. Int.* **111**, 253-266.
- Solomon, S. C. (1976). Sizes of ridge crest earthquakes and lithospheric thickness thickness at spreading centers (abstract), *Eos Trans. AGU* **57**, 954.
- Solomon, S. C., and N. Burr (1979). The relationship of source parameters of ridge-crest and transform earthquakes to the thermal structure of oceanic lithosphere, *Processes at Mid-Ocean Ridges*, *Tectonophysics* **55**, J. Franchetau (Editor), 107-126.

- Stein, S. (1993). Space geodesy and plate motions, in D.E. Smith & D. L. Turcotte, (editors), *Contributions of Space Geodesy to Geodynamics: Crustal Dynamics, Geodynamics Series*, **23**, Amer. Geophys. U., 5-20.
- Taymaz, T., J. Jackson, and R. Westaway (1990). Earthquake mechanisms in the Hellenic Trench near Crete, *Geophys J. Int.* **102**, 695–731.
- Tichelaar, B. W., and L. J. Ruff (1993) Depth of seismic coupling along subduction zones, *J. Geophys. Res.*, **98**, 2017-2038.
- Uyeda, S., and H. Kanamori (1979). Back-arc opening and the mode of subduction, *J. Geophys. Res.*, **84**, 1049-1061.
- van den Beukel, J., and R. Wortel (1987). Temperatures and shear stresses in the upper part of a subduction zone, *Geophys. Res. Lett.* **14**(10), 1057-1060.
- Vrolijk, P. (1990). On the mechanical role of smectite in subduction zones, *Geology* **18**(8), 703-707.

#### **Authors' affiliations, addresses**

- Peter Bird, Department of Earth and Space Sciences, University of California, Los Angeles, CA 90095-1567.
- Yan Y. Kagan, Department of Earth and Space Sciences, University of California, Los Angeles, CA 90095-1567.
- David D. Jackson, Department of Earth and Space Sciences, University of California, Los Angeles, CA 90095-1567.
- Frederic P. Schoenberg, Department of Statistics, University of California, Los Angeles, CA 90095-1554.

Maximilian J. Werner, Swiss Seismological Service, Eidgenössische Technische Hochschule,  
Zurich.

## Tables

**Table 1: Classes of plate boundary (Bird, 2003; Bird & Kagan, 2004)**

<b>Abbreviation</b>	<b>Class</b>	<b>Total length*, km</b>	<b>Mean* velocity, mm/a</b>	<b>Earthquake count*, <math>N...</math></b>	<b>above <math>M_t</math>, N m</b>
CCB	Continental Convergent Boundary	12516	18.2	300	$3.47 \times 10^{17}$
CRB	Continental Rift Boundary	18126	18.9	214	$3.47 \times 10^{17}$
CTF	Continental Transform Fault	19375	21.5	230	$3.47 \times 10^{17}$
OCB	Oceanic Convergent Boundary	13236	19.2	101	$3.47 \times 10^{17}$
OSR	Oceanic Spreading Ridge	61807	47.0	260	$2.07 \times 10^{17}$
OTF	Oceanic Transform Fault	43902	40.5	1285	$2.07 \times 10^{17}$
SUB	Subduction zone	38990	61.5	2057	$3.47 \times 10^{17}$

\*Total length, Mean velocity, and Earthquake count figures do not include any plate-boundary steps (or associated seismicity) within the 13 orogens of the PB2002 model.

## Figure Captions

Figure 1. Cumulative independent earthquake count (diamonds) and cumulative independent seismic moment (crosses) of Continental Transform Fault plate-boundary steps, ordered by relative plate velocity from slow on left to fast on right. Abscissa is cumulative model tectonic moment rate, assuming constant coupled seismogenic thickness, constant spectral slope, and constant corner magnitude. Diagonal reference line represents the null hypothesis of linearity.

Figure 2. Cumulative independent earthquake count (diamonds) and cumulative independent seismic moment (crosses) of Continental Rift Boundary plate-boundary steps, ordered by relative plate velocity. Conventions as in Figure 1.

Figure 3. Cumulative independent earthquake count (diamonds) and cumulative independent seismic moment (crosses) of Oceanic Transform Fault plate-boundary steps, ordered by relative plate velocity. Conventions as in Figure 1.

Figure 4. Cumulative independent earthquake count (diamonds) and cumulative independent seismic moment (crosses) of Oceanic Convergent Boundary plate-boundary steps, ordered by relative plate velocity. Conventions as in Figure 1.

Figure 5. Cumulative independent earthquake count (diamonds) and cumulative independent seismic moment (crosses) of Oceanic Spreading Ridge plate-boundary steps, ordered by relative plate velocity.

Figure 6. Cumulative independent earthquake count (diamonds) and cumulative independent seismic moment (crosses) of Subduction-zone plate-boundary steps, ordered by relative plate velocity.

Figure 7. Cumulative independent earthquake count (diamonds) and cumulative independent seismic moment (crosses) of Continental Convergence Zone plate-boundary steps, ordered by relative plate velocity.

Figure 8. “Slow” subduction zones ( $v < 67$  mm/a; heavy black lines) outside orogens (shading) from the PB2002 model of Bird (2003), who defined them as convergent boundaries with associated volcano(es) (triangles) and/or Wadati-Benioff zones of intermediate-depth seismicity (circles). Large asterisks indicate slow subduction zones that were not included in the “Subduction zone deformation regime” of Kreemer *et al.* (2002).

Earthquakes deeper than 70 km are from CMT and volcanoes are from Simkin & Siebert (1995).

Figure 9. Thermal structure of a vertical cross-section of a model subduction zone, after 100 m.y. of subduction at 60 mm/a. The F-D grid has been rotated for greater realism, as explained in text. Geotherms of the subducting oceanic plate (right) and the volcanic arc (left) were fixed as boundary conditions. Diagonal line indicates the interplate shear zone. Contour interval 50 C.

Figure 10. Depths (below seafloor) to various temperatures in the interplate shear zone, from F-D thermal models like that shown in Figure 9. The 150 C isotherm is suggested as an estimate of the lower limit of the (potentially) frictional and seismogenic portion of the shear zone.

Figure 11. Potentially seismogenic lithosphere thicknesses, expressed as depth extents of the (potentially) seismogenic portion of the interplate subduction shear zone. Obtained from Figure 10 by subtraction of a constant 12.4 km depth to the beginning of the seismogenic zone.

Figure 12. Estimated variations in corner magnitude of shallow subduction zone earthquakes due solely to velocity-dependent variations in thermal structure, as shown in Figures 10-11. Fixed point is the global average value of Bird & Kagan (2004), plotted at the relative plate velocity of the 1960 Chilean earthquake. In very slow subduction, plate-bending earthquakes may dominate the corner magnitude.

Figure 13. Global-average histograms of shallow earthquake counts, by focal mechanism, in subduction zones of the PB2002 model (outside designated orogens). Width of all bins is 10 km. Thrusting earthquakes located to the right of the trench probably did not occur on the interplate shear zone, but were due to plate bending. Some thrusting earthquakes to the left of the trench were also due to plate bending. By estimating that plate-bending produces equal numbers of normal and thrusting earthquakes, we compute the fraction of earthquakes taking place on the interplate shear zone to be  $100\% - 9.4\% - 2 \times 14.5\% = 62\%$ .

Figure 14. Normalized earthquake productivity (defined in text) variations predicted from the F-D thermal models of Figures 9-12, and the observed earthquake partitioning in subduction zones from Figure 13. Greater seismogenic lithosphere thickness at higher velocity is offset by the effect of higher corner magnitude, predicting roughly uniform productivity.

Figure 15. Potential extent of subducted evaporite sediments (white honeycomb pattern) based on present plate velocities from PB2002 (Bird, 2003) and an assumption that some evaporites travel at the velocity of the subducting plate (AF or EU). Evaporites under the Italian peninsula are hypothetical, and depend on both the past motion of the peninsula with respect to Adria (here based on Figure 6 of Rosenbaum *et al.*, 2008), and whether a suitably deep basin existed for Messinian evaporite formation off the former southwestern continental margin of the Adria microcontinent, prior to its collision with Italy.

Figure 16. Schematic diagram of possible conditions at intermediate depth (*e.g.*, 27 km below sea level) in an interplate subduction shear zone. The shear stress necessary to accommodate relative plate motion by viscous flow (solid lines) might increase linearly or according to a power-law. The shear stress necessary for frictional sliding (dashed curves) is controlled by pore pressure, whose sensitivity to plate velocity is unknown. Their intersection (at one of the 4 circled points) would divide low-velocity aseismic behavior from high-velocity seismic behavior at this particular point in the shear zone.

## Figure Captions & Figures

### CTF: Continental Transform Faults (no orogens)

CMT, 1982.01.01-2007.03.31,  $m > 5.66$ :  $N = 173.9$  independent / 230

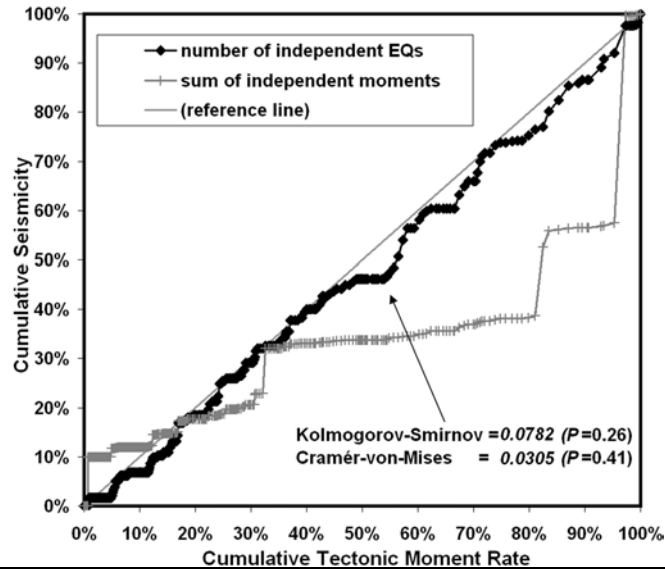


Figure 1. Cumulative independent earthquake count (black diamonds) and cumulative independent seismic moment (gray crosses) of Continental Transform Fault plate-boundary steps, ordered by relative plate velocity from slow on left to fast on right. Abscissa is cumulative model tectonic moment rate, assuming constant coupled seismogenic thickness, constant spectral slope, and constant corner magnitude. Diagonal reference line represents the null hypothesis of linearity.

### CRB: Continental Rift Boundaries (no orogens)

CMT, 1982.01.01-2007.03.31,  $m > 5.51$ :  $N = 172.1$  independent / 214

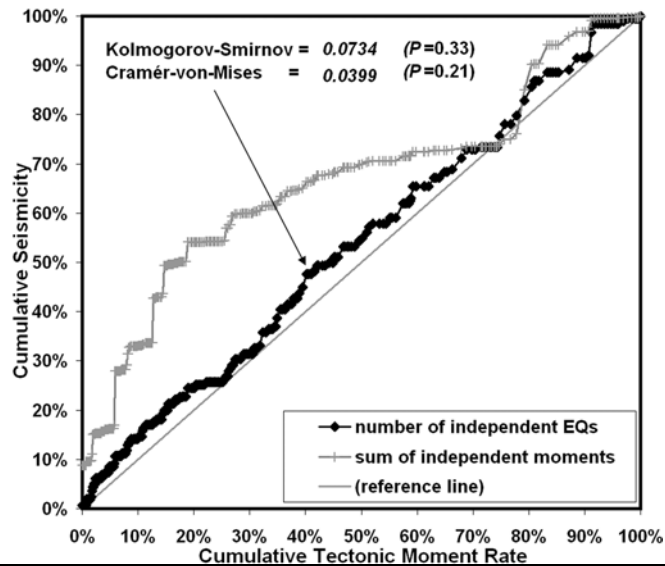


Figure 2. Cumulative independent earthquake count (black diamonds) and cumulative independent seismic moment (gray crosses) of Continental Rift Boundary plate-boundary steps, ordered by relative plate velocity. Conventions as in Figure 1.

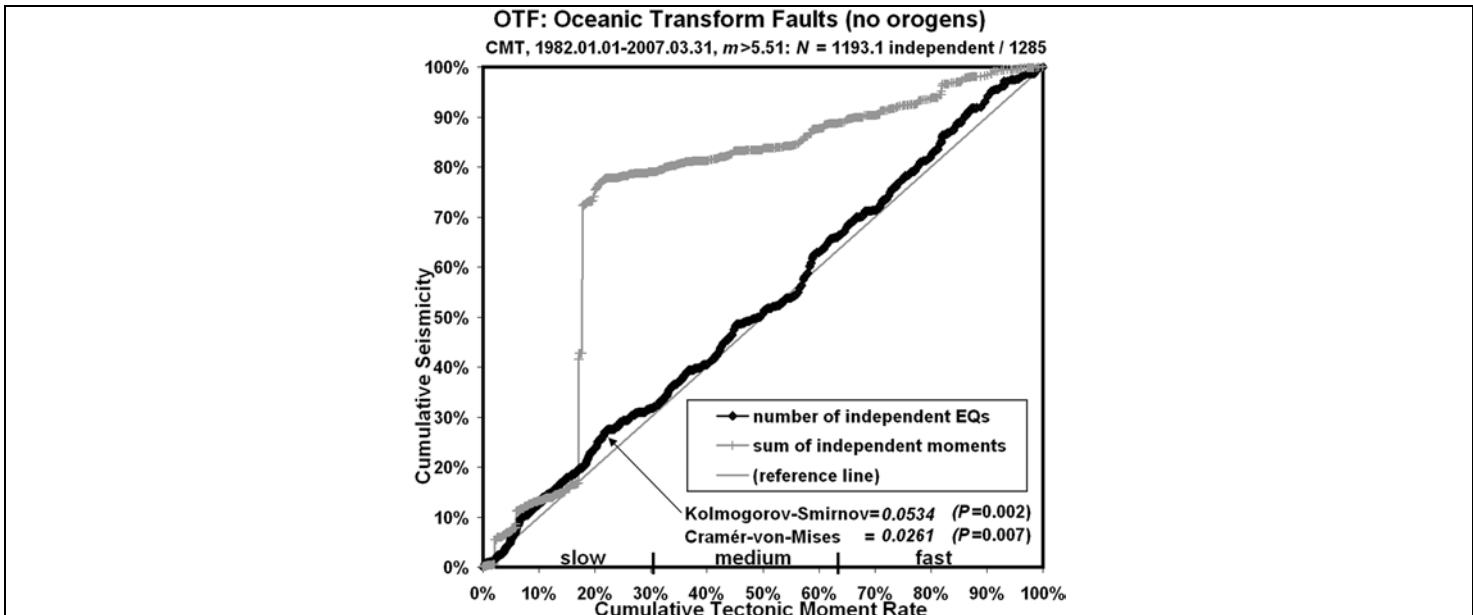


Figure 3. Cumulative independent earthquake count (black diamonds) and cumulative independent seismic moment (gray crosses) of Oceanic Transform Fault plate-boundary steps, ordered by relative plate velocity. Conventions as in Figure 1.

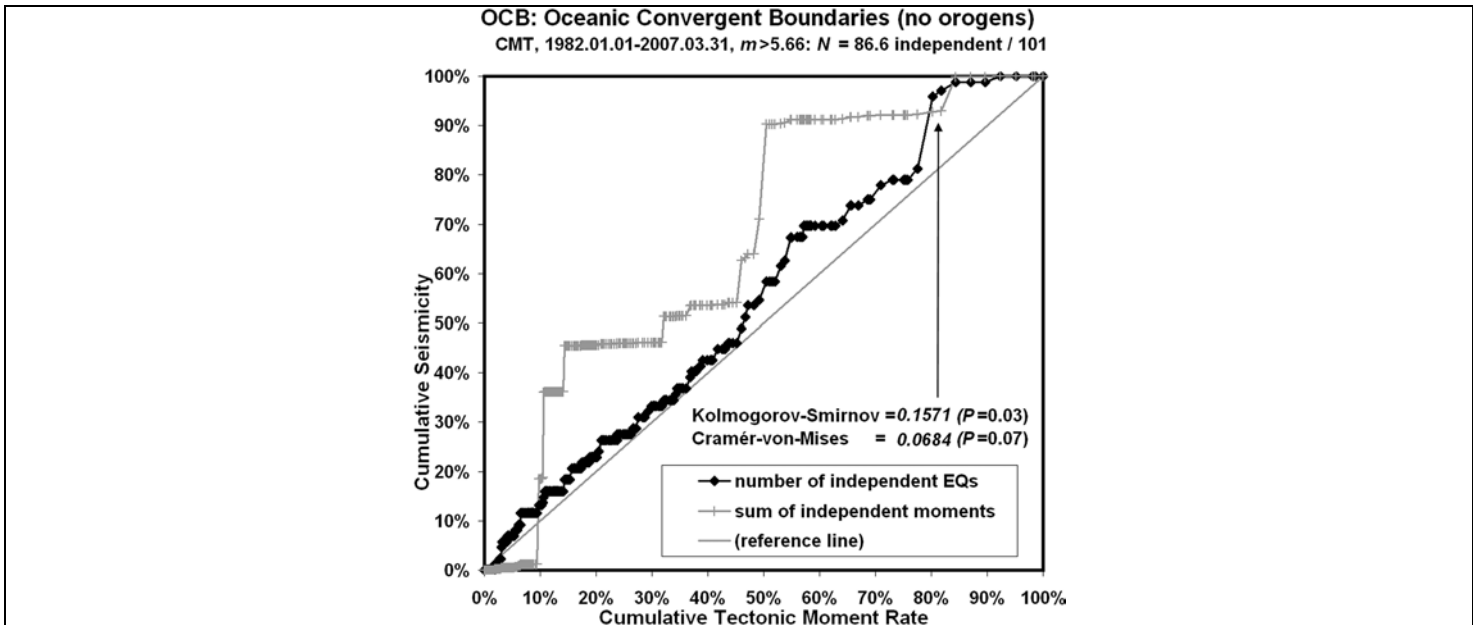


Figure 4. Cumulative independent earthquake count (black diamonds) and cumulative independent seismic moment (gray crosses) of Oceanic Convergent Boundary plate-boundary steps, ordered by relative plate velocity. Conventions as in Figure 1.

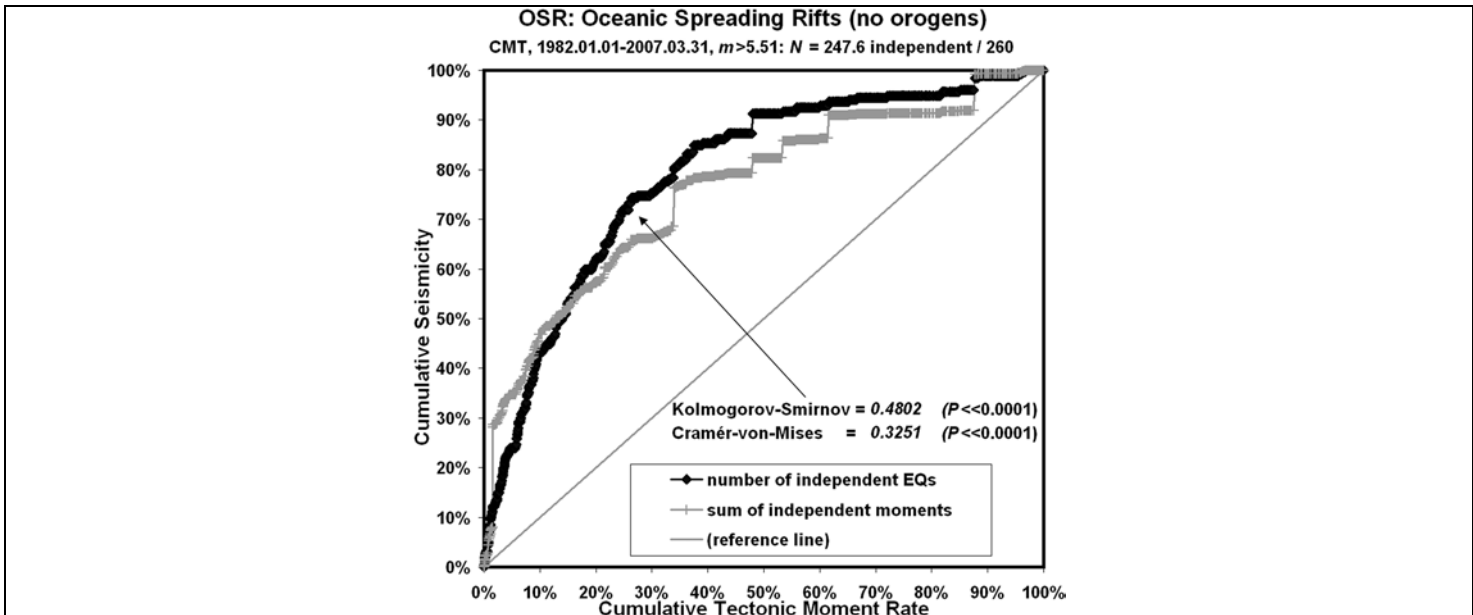


Figure 5. Cumulative independent earthquake count (black diamonds) and cumulative independent seismic moment (gray crosses) of Oceanic Spreading Ridge plate-boundary steps, ordered by relative plate velocity.

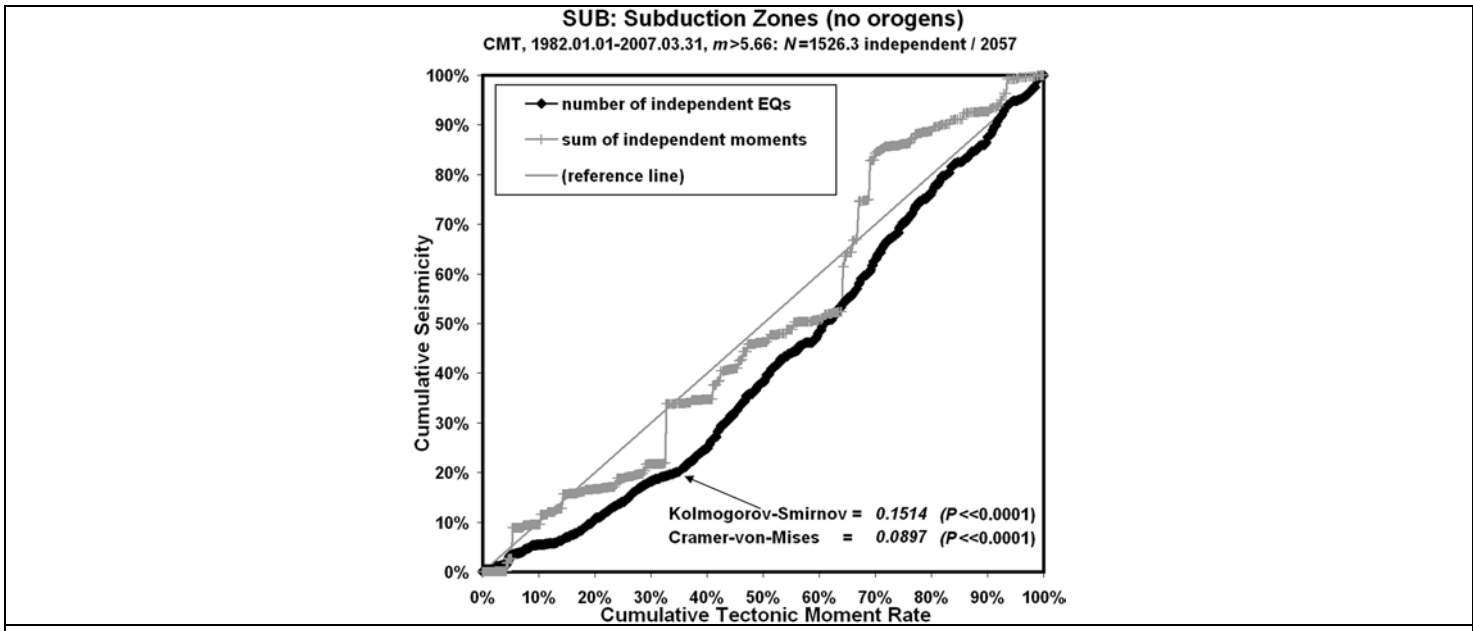


Figure 6. Cumulative independent earthquake count (black diamonds) and cumulative independent seismic moment (gray crosses) of Subduction-zone plate-boundary steps, ordered by relative plate velocity.

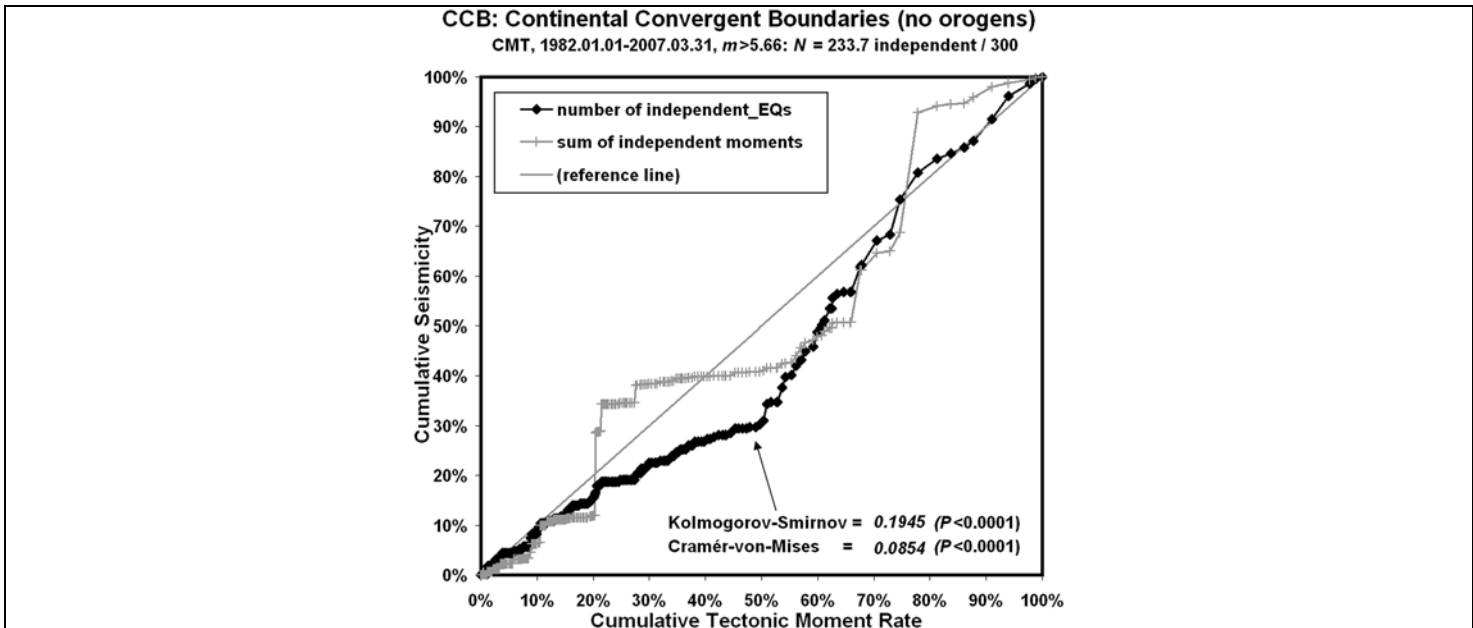


Figure 7. Cumulative independent earthquake count (black diamonds) and cumulative independent seismic moment (gray crosses) of Continental Convergence Zone plate-boundary steps, ordered by relative plate velocity.

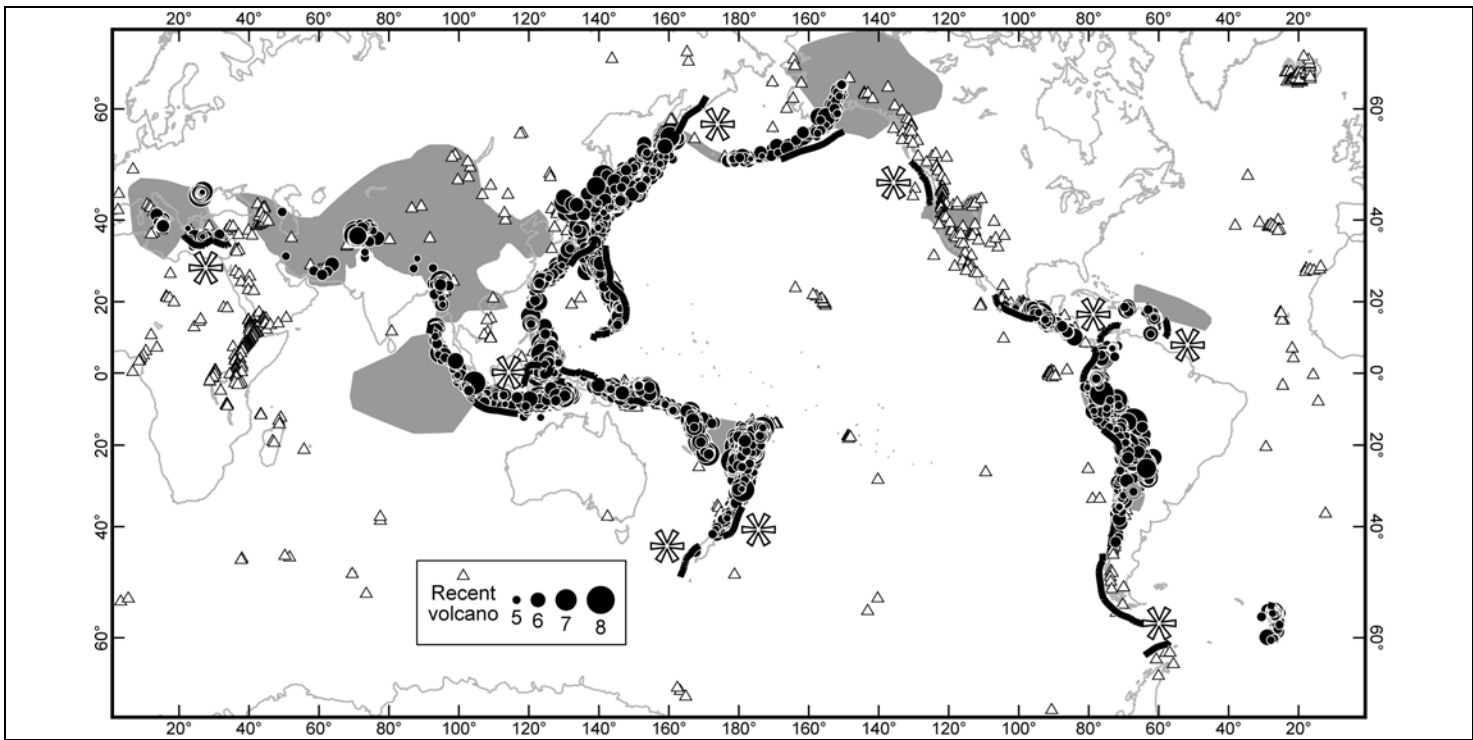


Figure 8. “Slow” subduction zones ( $v < 67$  mm/a; heavy black lines) outside orogens (shading) from the PB2002 model of Bird (2003), who defined them as convergent boundaries with associated volcano(es) (triangles) and/or Wadati-Benioff zones of intermediate-depth seismicity (circles). Large asterisks indicate slow subduction zones that were not included in the “Subduction zone deformation regime” of Kreemer *et al.* (2002). Earthquakes deeper than 70 km are from CMT, and volcanoes are from Simkin & Siebert (1995).

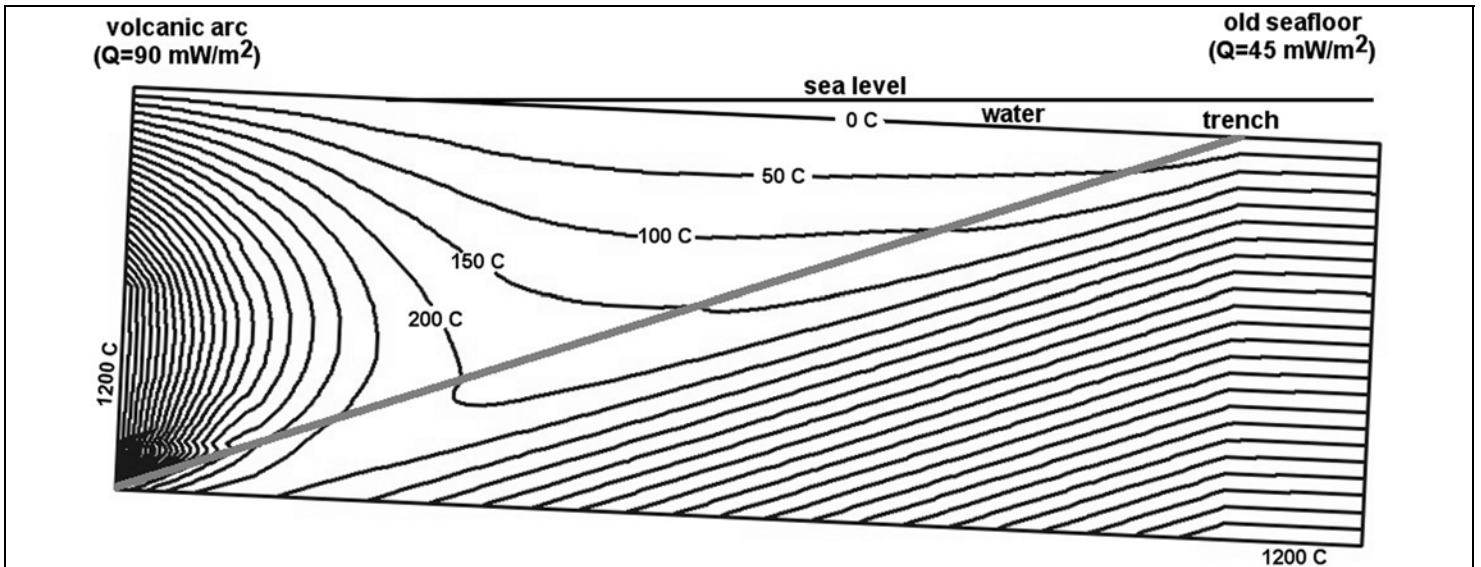


Figure 9. Thermal structure of a vertical cross-section of a model subduction zone, after 100 m.y. of subduction at 60 mm/a. The F-D grid has been rotated for greater realism, as explained in text. Geotherms of the subducting oceanic plate (right) and the volcanic arc (left) were fixed as boundary conditions. Diagonal line indicates the interplate shear zone. Contour interval 50 C.

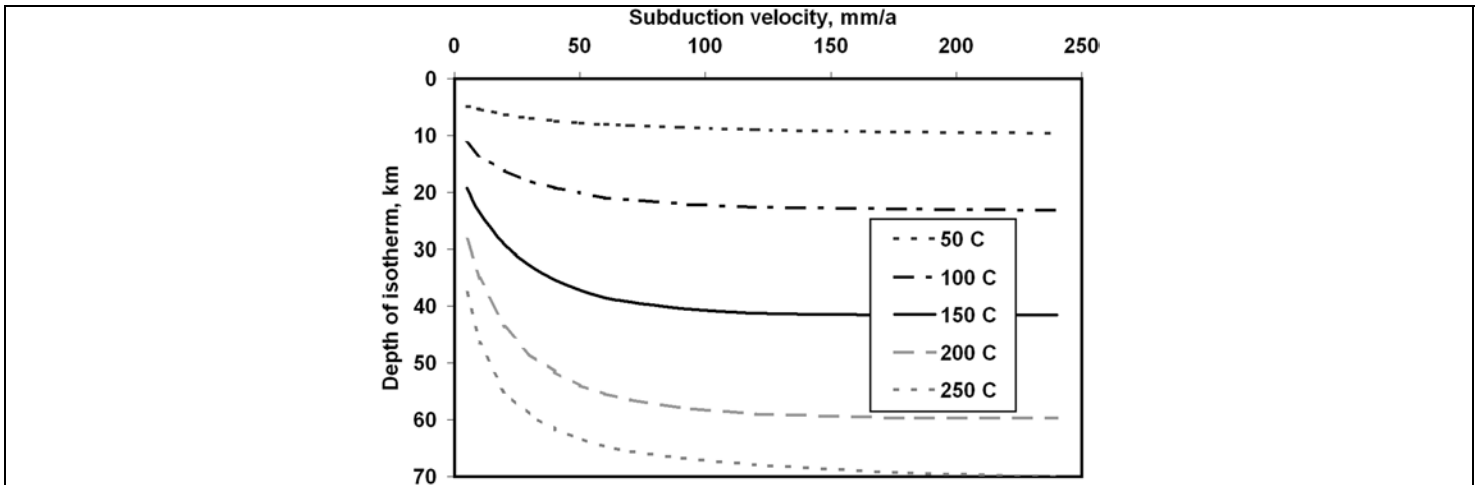


Figure 10. Depths (below seafloor) to various temperatures in the interplate shear zone, from F-D thermal models like that shown in Figure 9. The 150 C isotherm is suggested as an estimate of the lower limit of the (potentially) frictional and seismogenic portion of the shear zone.

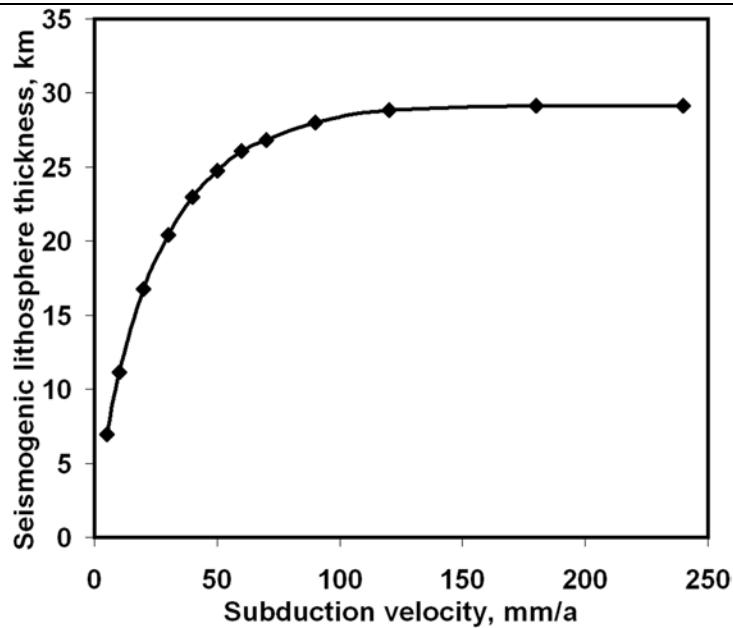


Figure 11. Potentially seismogenic lithosphere thicknesses, expressed as depth extents of the (potentially) seismogenic portion of the interplate subduction shear zone. Obtained from Figure 10 by subtraction of a constant 12.4 km depth to the beginning of the seismogenic zone.

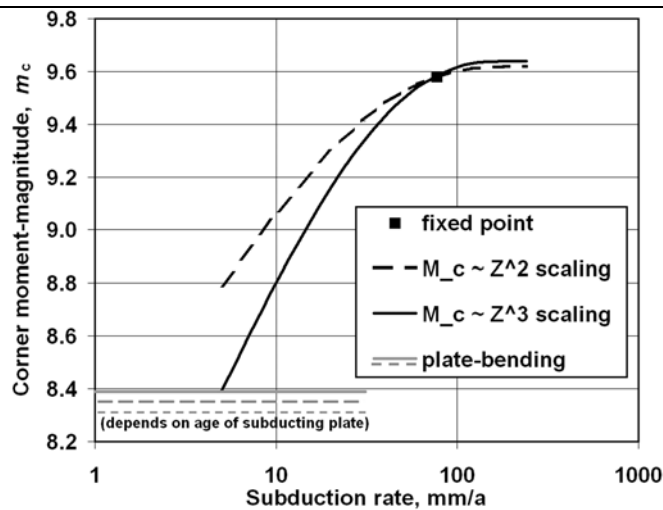


Figure 12. Estimated variations in corner magnitude of shallow subduction zone earthquakes due solely to velocity-dependent variations in thermal structure, as shown in Figures 10-11. Fixed point is the global average value of Bird & Kagan (2004), plotted at the relative plate velocity of the 1960 Chilean earthquake. In very slow subduction, plate-bending earthquakes may dominate the corner magnitude.

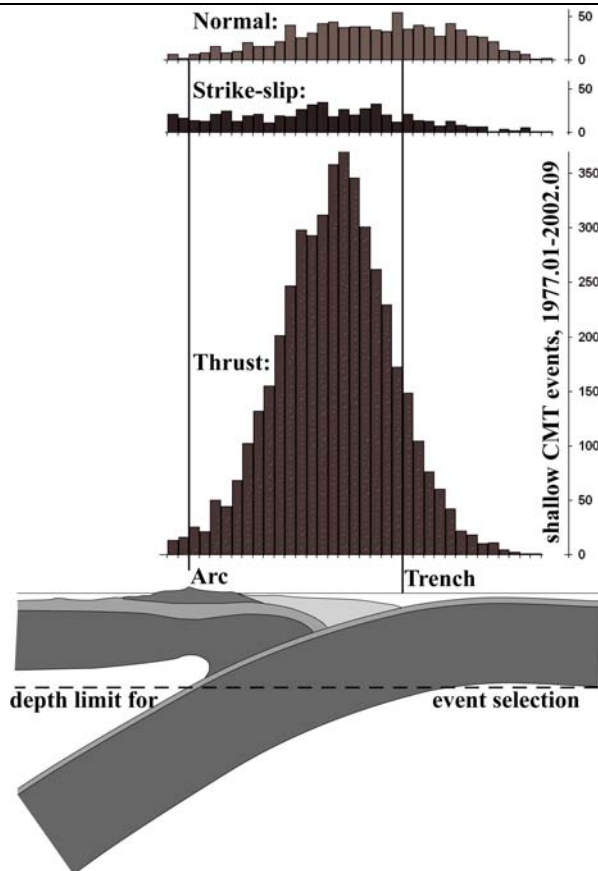


Figure 13. Global-average histograms of shallow earthquake counts, by focal mechanism, in subduction zones of the PB2002 model (outside designated orogens). Width of all bins is 10 km. Thrusting earthquakes located to the right of the trench probably did not occur on the interplate shear zone, but were due to plate bending. Some thrusting earthquakes to the left of the trench were also due to plate bending. By estimating that plate-bending produces equal numbers of normal and thrusting earthquakes, we compute the fraction of earthquakes taking place on the interplate shear zone to be  $100\% - 9.4\% - 2 \times 14.5\% = 62\%$ .

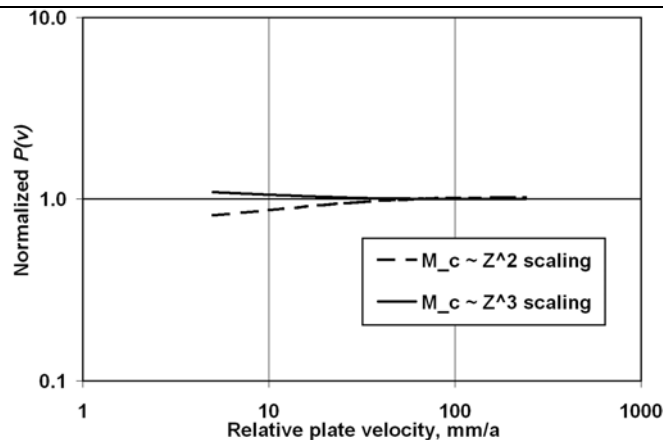


Figure 14. Normalized earthquake productivity (defined in text) variations predicted from the F-D thermal models of Figures 9-12, and the observed earthquake partitioning in subduction zones from Figure 13. Greater seismogenic lithosphere thickness at higher velocity is offset by the effect of higher corner magnitude, predicting roughly uniform productivity.

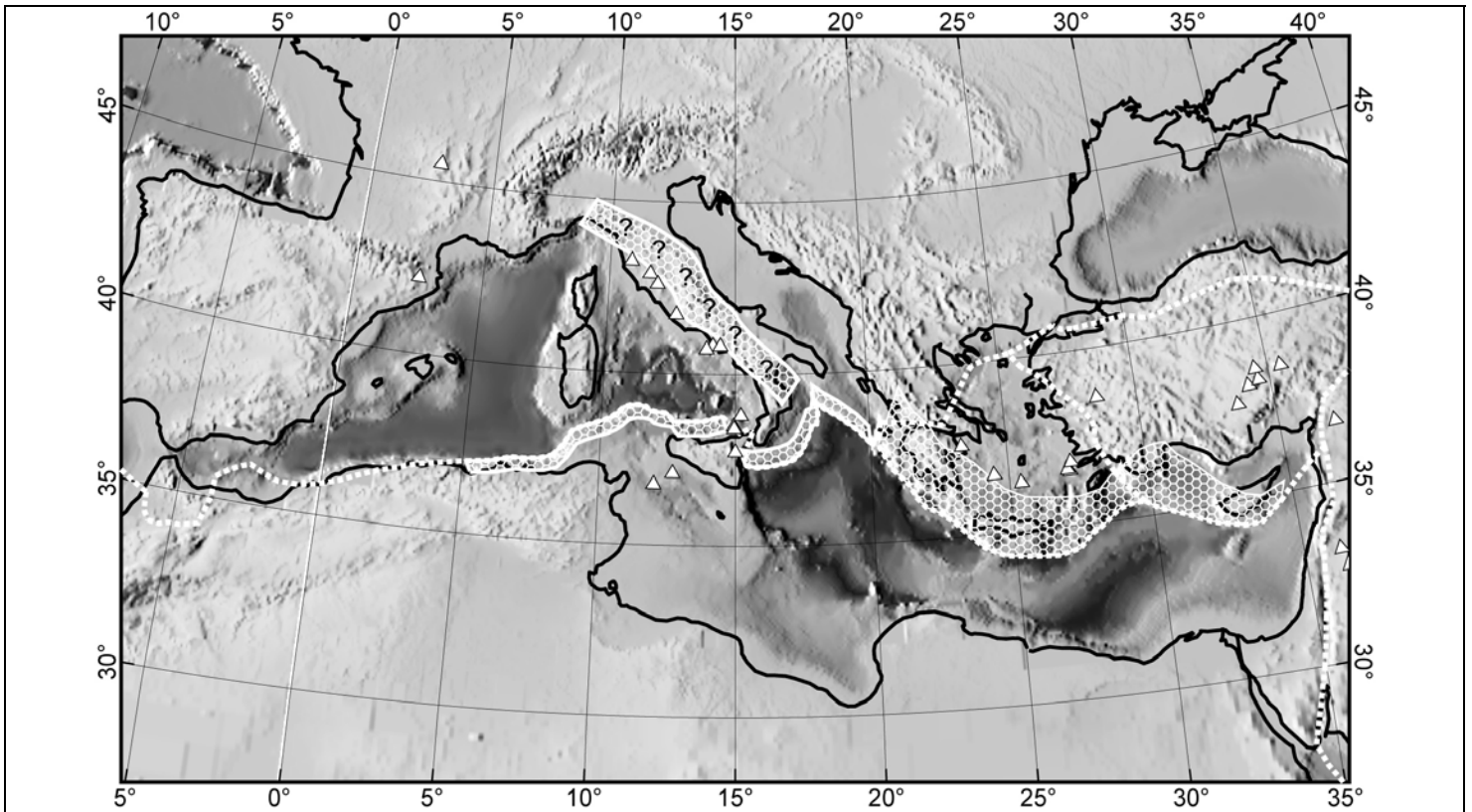


Figure 15. Potential extent of subducted evaporite sediments (white honeycomb pattern) based on present plate velocities from PB2002 (Bird, 2003) and an assumption that some evaporites travel at the velocity of the subducting plate (AF or EU). Evaporites under the Italian peninsula are hypothetical, and depend on both the past motion of the peninsula with respect to Adria (here based on Figure 6 of Rosenbaum *et al.*, 2008), and whether a suitably deep basin existed for Messinian evaporite formation off the former southwestern continental margin of the Adria microcontinent, prior to its collision with Italy.

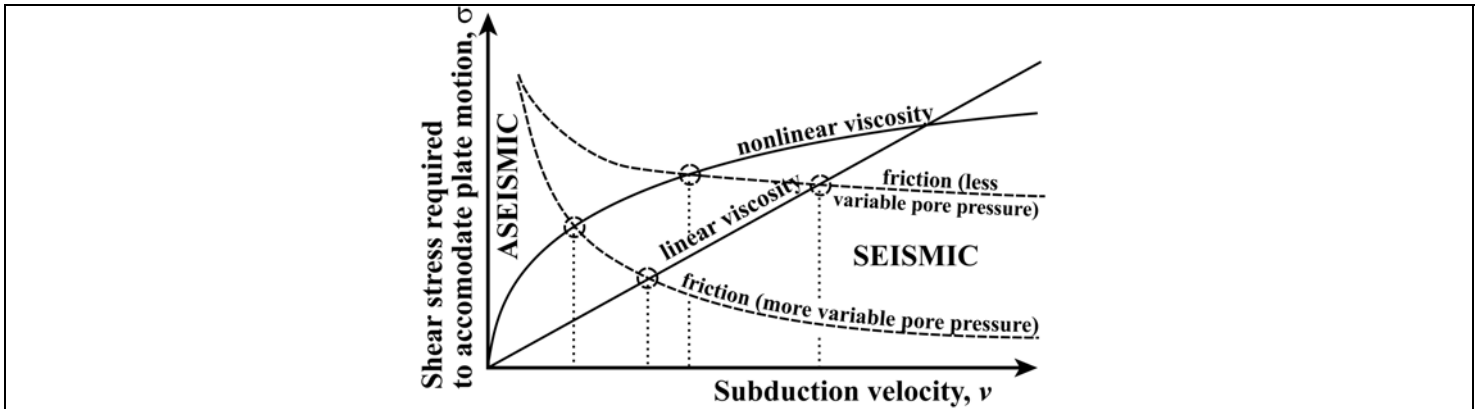


Figure 16. Schematic diagram of possible conditions at intermediate depth (*e.g.*, 27 km below sea level) in an interplate subduction shear zone. The shear stress necessary to accommodate relative plate motion by viscous flow (solid lines) might increase linearly or according to a power-law. The shear stress necessary for frictional sliding (dashed curves) is controlled by pore pressure, whose sensitivity to plate velocity is unknown. Their intersection (at one of the 4 circled points) would divide low-velocity aseismic behavior from high-velocity seismic behavior at this particular point in the shear zone.